Table 1. The sequences of gene-specific primers for reverse transcriptase–polymerase chain reaction (RT-PCR) and real-time RT-PCR used in this study

Primer	Sequence
IL-4 forward	CACAGGCACAAGCAGCTGAT
IL-4 reverse	CCTTCACAGGACAGGAATTCAAG
IL-6 forward	GTAGCCGCCCCACACAGA
IL-6 reverse	CCGTCGAGGATGTACCGAAT
IL-10 forward	GCCAAGCCTTGTCTGAGATGA
IL-10 reverse	CTTGATGTCTGGGTCTTGGTTCT
IL-17 forward	GACTCCTGGGAAGACCTCATTG
IL-17 reverse	TGTGATTCCTGCCTTCACTATGG
IL-17F forward	GCTTGACATTGGCATCATCAA
IL-17F reverse	GGAGCGGCTCTCGATGTTAC
IL-23 forward	GAGCCTTCTCTGCTCCCTGATAG
IL-23 reverse	AGTTGGCTGAGGCCCAGTAG
IL-23R forward	AACAACAGCTCGGCTTTGGTATA
IL-23R reverse	GGGACATTCAGCAGTGCAGTAC
IFNG forward	CATCCAAGTGATGGCTGAACTG
IFNG reverse	TCGAAACAGCATCTGACTCCTTT
GM-CSF forward	CAGCCCTGGAGCATGTG
GM-CSF reverse	CATCTCAGCAGCAGTGTCTCTAC^{r}
RORγt forward	TGGGCATGTCCCGAGATG
RORγt reverse	GCAGGCTGTCCCTCTGCTT
STAT-3 forward	GGAGGAGGCATTCGGAAAGT
STAT-3 reverse	GCGCTACCTGGGTCAGCTT
FOXP3 forward	GAGAAGCTGAGTGCCATGCA
FOXP3 reverse	GCCACAGATGAAGCCTTGGT

IL, interleukin; *IFNG*, interferon γ; *FOXP3*, forkhead box protein 3; *GM-CSF*, granulocyte–macrophage colony-stimulating factor; *RORγt*, retinoic acid receptor-related orphan receptor γ isoform t; *STAT*, signal transducer and activator of transcription.

transcribed and labelled using One-Cycle Target Labeling and Control Reagents as instructed by the manufacturer (Affymetrix, Santa Clara, CA). The labelled probes were hybridized to a Human Genome U133 Plus 2·0 Array (Affymetrix). The arrays were used in a single experiment and analysed with GENECHIP operating software 1.2 (Affymetrix). Background subtraction and normalization were performed using GENESPRING GX 7.3 software (Agilent Technologies, Santa Clara, CA). The signal intensity was pre-normalized based on the positive control genes (GAPDH and β-actin) for all measurements on that chip. To account for differences in detection efficiency between spots, the pre-normalized signal intensity of each gene was normalized to the median of pre-normalized measurements for that gene. The data were filtered as follows. (i) Genes that were scored as absent in all samples were eliminated. (ii) Genes with a signal intensity of < 90 were eliminated. (iii) Genes that exhibited increased (fold-change > 2) or decreased (fold-change > 2) expression in CB-derived $CD4^+$ T cells compared with PB-derived $CD4^+$ T cells were selected by comparing the mean value of signal intensities in each condition.

Immunofluorescence study

After periods of cultivation, cells were collected and stained with fluorescence-labelled monoclonal antibodies and analysed by flow cytometry (FC500; Beckman/Coulter, Fullerton, CA). A four-colour immunofluorescence study was performed with a combination of fluorescein isothiocyanate (FITC)-conjugated anti-CD3, phycoerythrin (PE)-conjugated anti- forkhead box protein 3 (Foxp3), phycoerythrin-cyanine-5 (PC5)-conjugated anti-CD4 and PC7-conjugated anti-CD8 (Beckman/Coulter). After staining of cell surface antigens, cells were permeabilized with IntraPrep (Dako, Glostrup, Denmark) and intracellular antigen (Foxp3) was further stained.

Statistical analysis

The statistical analysis was performed using a Student's *t*-test and a *P*-value $< 0{\cdot}05$ was considered to be statistically significant.

Results

Expression profiles of activated $CD4^+$ T cells derived from human CB and PB

To compare the gene expression patterns of CB-derived $CD4^+$ cells and PB-derived $CD4^+$ cells, we performed DNA microarray analysis using the Affymetrix Human Genome U133 Plus 2·0 Array. After background subtraction, comparison of the gene expression profiles of two independent CB-derived $CD4^+$ samples and PB-derived $CD4^+$ samples was performed using a gene cluster analysis. The genes differentially expressed (fold-change > 2) between the activated $CD4^+$ T cells derived from CB and those derived from PB were selected, and 396 probes were found to exhibit higher levels of expression in CB-derived $CD4^+$ samples while 131 probes exhibited higher levels in PB-derived $CD4^+$ samples. Parts of the data are summarized and presented in Fig. 1a and Tables 2–4.

Among these genes, those closely correlated to T-cell function and development were selected (Fig. 1b). The genes exhibiting higher levels of expression in CB-derived $CD4^+$ samples included those encoding cell cycle regulators, including cyclin-dependent kinase (CDKN)2A and 2B, transcriptional regulators and signal transduction factors (Tables 2 and 3). The genes for cytokines, chemokines and their receptors such as Interferon γ (IFNG), granulocyte-macrophage colony-stimulating factor (GM-CSF) and for T-cell transcriptional regulators (*FOXP3*) as well as the genes related to T-cell development including CD28, cytotoxic T lymphocyte antigen-4 (CTLA4) and inducible T-cell co-stimulator (ICOS) were also found among the genes exhibiting higher levels of expression in CB-derived $CD4^+$ samples (Fig. 1b). The factors reported

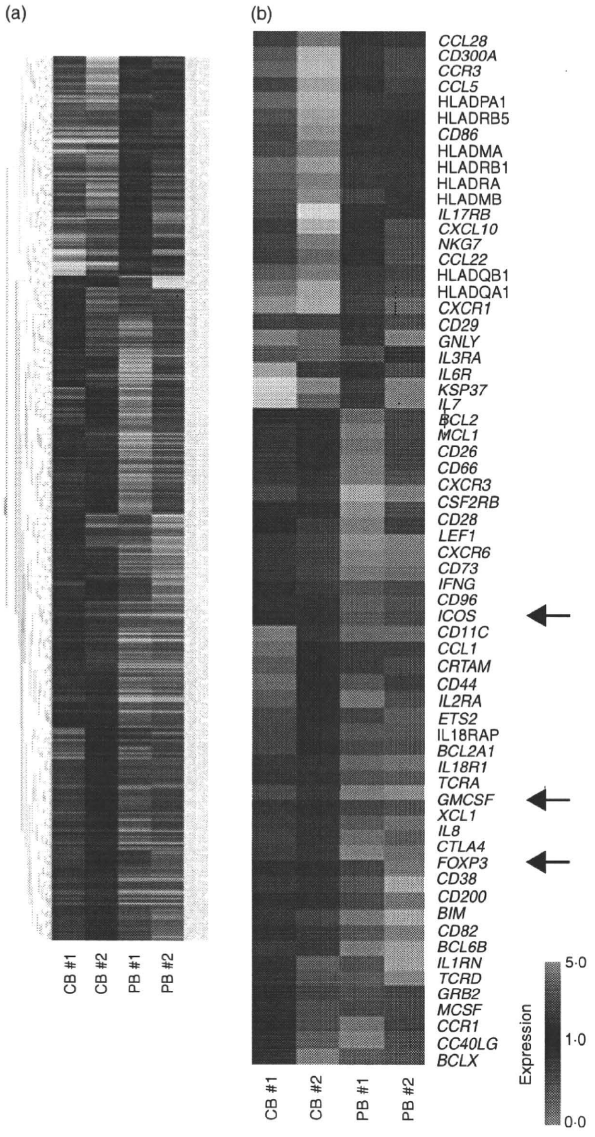

Figure 1. Comparison of the gene expression profiles of cord blood (CB)- and peripheral blood (PB)-derived $CD4^+$ T cells. Hierarchical clustering of results from a microarray analysis for CB- and PB-derived $CD4^+$ T cells is indicated. (a) A total of 529 genes characterizing $CD4^+$ T cells (396 genes for CB-derived $CD4^+$ T cells and 131 genes for PB-derived $CD4^+$ T cells) were used to create the gene tree. The gene list is presented in Tables 3 and 4. (b) Genes related to T-cell development (40 genes for CB-derived $CD4^+$ T cells and 26 genes for PB-derived $CD4^+$ T cells) are presented. The arrows indicate the expression pattern of T-cell lineage-specific genes including inducible T-cell co-stimulator (*ICOS*), granulocyte-macrophage colony-stimulating factor (*GM-CSF*) and forkhead box protein 3 (*FOXP3*).

to be essential for negative selection in $CD4^+$ $CD8^+$ thymocytes such as BCL2-like 11 (BIM)[10] as well as other apoptotic regulators were also found among the genes exhibiting higher expression levels in CB-derived $CD4^+$ samples.

The genes with a higher level of expression in the PB-derived $CD4^+$ T cells included those encoding transcriptional regulators, signal transduction factors, major histocompatibility complex (MHC) class II molecules (*HLADMA*, *HLADMB*, *HLADPA1*, *HLADQB1*, *HLADRA*, *HLADRB1* and *HLADRB5*), and cytokines, chemokines and their receptors (*IL-7*, *IL-17RB*), as well as genes that characterize the T-cell lineage (*CD29*, *CD86*) (Fig. 1b, Tables 2, 4).

Notably, microarray studies showed that the expression of several regulatory T cell (Treg)-related genes was significantly higher in the CB-derived T cells. Foxp3 is an important T-cell transcription factor and is considered to be a marker of Tregs. Cytotoxic T-lymphocyte antigen-4 (CTLA-4) and ICOS, which belong to the CD28 family of receptors and play a crucial role in the activation of T cells, were reported to be highly expressed in activated Tregs.[11,12] All of the above genes were expressed at higher levels in the CB-derived CD4 T cells (Fig. 1).

The microarray results for major genes related to the development of the T-cell lineage, including those not appeared in Fig. 1, are summarized in Table 2. As shown in Table 2, the expression of T-cell lineage master regulator genes, such as *TBX21*, *GATA3* and *MAF*, and T cell-related cytokines, such as *IL-4*, *IL-5*, *IL-13*, *IL-22* and *TGFB1*, revealed no significant difference between CB-derived $CD4^+$ cells and PB-derived $CD4^+$ cells. However, other T cell-related genes, including *IL-2*, *IL-6*, *IL-9*, *IL-10* and *IL-17*, were eliminated from the list in the course of background subtraction because the signal intensity of each gene was low (< 90 as raw data) in all of the samples.

Differences in the expression patterns of T-cell lineage-specific genes between CB-derived and PB-derived $CD4^+$ T cells

To further confirm the characteristic gene expression in CB- and PB-derived $CD4^+$ T cells, we performed a real-time RT-PCR analysis. Consistent with the microarray data, when the mRNA levels of the genes related to the T helper type 1 (Th1) and Th2 phenotypes were examined, higher levels of GM-CSF and IFNG were observed in CB-derived T cells, while IL-4 revealed no significant tendency (Fig. 2). We also examined IL-6 and IL-10 and no significant tendency was observed either in the expression of these genes (Fig. 2).

Next we examined the expression of the genes related to Tregs and observed a higher level of Foxp3, but lower levels of retinoic acid receptor-related orphan receptor γ isoform t (RORγt); and IL-17F, in CB-derived T cells (Fig. 3). In contrast, there was no significant tendency in the expression of genes encoding signal transducer and activator of transcription 3 (STAT-3), IL-23 and IL-23 receptors. In the case of the *IL-17* gene, clear amplifica-

Table 2. The microarray results for T-cell-related genes

Description	Gene	Gene ID	CB-1		CB-2		PB-1		PB-2	
			Normalized	Raw	Normalized	Raw	Normalized	Raw	Normalized	Raw
Master regulation										
Thl	*TBX21*	220684_at	1·1382915	305·7	0·7851455	247·1	1·045663	230·5	0·954337	261·4
Th2	*GATA3*	209602_s_at	1·471558	1204	0·7742825	742·1	1·0740323	721·1	0·9259675	772·5
	GATA3	209603_at	1·265932	416·5	0·53335179	205·7	1·0535141	284·5	0·9464856	317·6
	GATA3	209604_s_at	1·350573	5300	0·6415387	2950	1·0573606	3406	0·9426395	3773
	MAF	206363_at	0·7447395	672·7	0·8744312	925·6	1·1255689	834·5	1·2704437	1170
	MAF	209348_s_at	1·0320604	2078	0·8329663	1965	0·9679398	1600	1·8301903	3758
	MAF	229327_s_at	0·9099149	569·7	0·6089576	446·8	1·090085	560·2	1·4076804	898·9
Treg	*FOXP3*	221334_s_at	1·8893701	100·6	1·4199468	88·6	0·4988136	21·8	0·5800531	31·5
	FOXP3	224211_at	1·6205869	152·3	1·4101433	155·3	0·5898568	45·5	0·2347433	22·5
Cytokines										
Thl	*IFNG*	210354_at	1·4801383	2000	1·9182948	3037	0·457517	507·4	0·5198616	716·4
	GM-CSF	210229_s_at	1·2802086	1293	2·6726868	3163	0·6906437	572·5	0·7197912	741·4
Th2	*IL-4*	207538_at	2·0291064	687·2	0·3361219	133·4	0·9317174	259	1·0682826	369
	IL-4	207539_s_at	2·8263247	965	0·3561467	142·5	0·8481774	237·7	1·1518226	401·1
	IL-5	207952_at	1·3380713	810	0·0610382	43·3	1·0097023	501·7	0·9902797	611·4
	IL-13	207844_at	3·9835246	1712	0·8117443	408·8	1·1453367	404	0·8691162	452·9
Treg	*TGFB1*	203085_s_at	1·5166419	774·9	0·9012154	539·6	1·0987847	460·8	0·8546632	374·6
Others	*IL-22*	222974_at	0·1272062	5·2	4·325279	207·2	0·5632869	18·9	1·4367131	59·9
Surface molecules										
Treg	*CTLA4*	231794_at	1·3871489	336·9	1·2560804	357·5	0·7439196	148·3	0·4444751	110·1
	CTLA4	236341_at	1·2573498	905·7	1·6210791	1368	0·6800935	402·1	0·7426501	545·6
Others	*IL-2RA*	206341_at	1·5216751	3569	1·2715347	3494	0·7284654	1402	0·6569936	1571
	IL-2RA	211269_s_at	1·1563299	4436	1·3173387	5923	0·8436702	2657	0·560745	2194
	ICOS	210439_at	1·378036	619·8	1·343834	708·3	0·567216	209·4	0·656166	301
	CD28	211856_x_at	1·3887135	144·9	1·2905376	157·8	0·3292731	28·2	0·7094624	75·5
	CD28	211861_x_at	1·350062	183·3	1·4109998	224·5	0·4863549	54·2	0·649938	90

The microarray results for major genes related to the development of the T-cell lineage are summarized. The normalized and raw data for four samples are indicated for each gene. Those for which differential expression was found between cord blood (CB)- and peripheral blood (PB)-derived $CD4^+$ T cells in a gene cluster analysis (fold-change > 2) are highlighted in grey. Genes exhibiting low signal intensity (< 90 as raw data) in all of the four samples were eliminated from the list beforehand in the process of background subtraction, and thus do not appeared in this table.

CTLA-4, cytotoxic T-lymphocyte antigen-4; *FOXP3*, forkhead box protein 3; GATA, GATA family of zinc finger trancription factors; *GM-CSF*, granulocyte–macrophage colony-stimulating factor; ICOS, inducible T-cell co-stimulator; IFNG, interferon γ; *IL*, interleukin; MAF, macrophage-activating factor; TBX21, T-box protein 21; TGFB1, transforming growth factor, beta 1; Th1, T helper type 1; Treg, regulatory T cell.

tion was detected in PB-derived T cells whereas no amplification was observed in the samples of CB-derived T cells (data not shown).

To further investigate whether increased expression of the *FOXP3* gene is a general feature of CB-derived $CD4^+$ T cells, we tested four samples of CB-derived $CD4^+$ T cells by real-time RT-PCR analysis and compared the results with those for equivalent numbers of PB-derived samples. As shown in Fig. 4, two CB-derived samples (CB 4 and 5, at 2 weeks) revealed significantly increased gene expression of *FOXP3* when compared with PB-derived samples, whereas the remaining two samples (CB 3 and 6; termed 'additional' samples below) did not. We also tested *FOXP3* gene expression at an earlier time-point in the same samples and observed no significant increase of *FOXP3* gene expression in CB-derived $CD4^+$ T cells at 1 week (Fig. 4). When the data were analysed statistically, expression of the *FOXP3* gene was found to be significantly higher in CB-derived $CD4^+$ T cells in comparison with equivalent PB-derived $CD4^+$ T cells at both 1 week ($P < 0{\cdot}05$) and 2 weeks ($P < 0{\cdot}05$) (Fig. 4).

Next we assessed the expression of the Foxp3 protein in CB-derived $CD4^+$ T cells. When the same samples as described above were examined by flow cytometry using a specific antibody, the Foxp3 protein was certainly detected in a portion of cells in all of four CB-derived samples while not detected in any of the PB-derived samples tested (Fig. 5). Inconsistent with the results of real-time RT-PCR, expression level of Foxp3 proteins was higher in CB-derived $CD4^+$ T cells at 1 week than at 2 weeks.

Table 3. Genes up-regulated in $CD4^+$ T cells from cord blood samples 1 and 2 (CB 1 and CB 2, respectively)

		Fold change				
Affi ID	Gene abbreviation	CB 1	CB 2	PB 1	PB 2	Gene name
Apoptosis						
1555372_at	*BimL*	1·39	1·52	0·61	0·42	BCL2-like 11 (apoptosis facilitator)
237837_at	*BCL2*	1·27	1·32	0·49	0·73	B-cell CLL/lymphoma 2
205681_at	*BCL2A1*	1·91	1·53	0·39	0·47	BCL2-related protein A1
1558143_a_at	*BCL2L11*	1·68	1·74	0·32	0·32	BGL2-like 11 (apoptosis facilitator)
228311_at	*BCL6B*	1·36	3·39	0·64	0·26	B-cell CLL/lymphoma 6, member B (zinc finger protein)
215037_s_at	*BCLX*	2·56	1·27	0·73	0·56	BCL2-like 1
224414_s_at	*CARD6*	2·65	1·34	0·56	0·66	Caspase recruitment domain family, member 6
201631_s_at	*IER3*	1·62	2·95	0·38	0·31	Immediate early response 3
218000_s_at	*PHLDA1*	2·34	1·21	0·53	0·79	Pleckstrin homology-like domain, family A, member 1
209803_s_at	*PHLDA2*	2·87	1·32	0·31	0·68	Pleckstrin homology-like domain, family A. member 2
203063_at	*PPMIF*	1·26	1·53	0·74	0·64	Protein phosphatase IF (PP2C domain containing)
205214_at	*STK17B*	1·78	1·26	0·74	0·71	Serine/threonine kinase 17b (apoptosis-inducing)
217853_at	*TENS1*	1·63	6·00	0·04	0·37	Tensin 1
B- and T-cell development						
211861_x_at	*CD28*	1·35	1·41	0·49	0·65	CD28 antigen(Tp44)
207892_at	*CD40LG*	3·67	1·32	0·45	0·68	C040 ligand (TNF superfamily, member 5, hyper-IgM syndrome)
206914_at	*CRTAM*	2·76	1·60	0·40	0·36	Class I MHC-restricted T-cell-associated molecule
210557_x_at	*CSF1*	3·79	1·22	0·78	0·70	Colony-stimulating factor 1 (macrophage)
210229_s_at	*CSF2*	1·28	2·67	0·69	0·72	Colony-stimulating factor 2 (granulocyte–macrophage)
205159_at	*CSF2RB*	2·33	1·60	0·18	0·40	Colony-stimulating factor 2 receptor
231794_at	*CTLA4*	1·39	1·26	0·74	0·44	Cytotoxic T-lymphocyte-associated protein 4
204232_at	*FCER1G*	1·63	2·14	0·28	0·37	Fc fragment of IgE, high affinity 1, receptor for; gamma polypeptide
210439_at	*ICOS*	1·38	1·34	0·57	0·66	Inducible T-cell costimulator
210354_at	*IFNG*	1·48	1·92	0·46	0·52	Human mRNA for HuIFN -gamma interferon
230536_at	*PBX4*	1·48	1·26	0·50	0·74	Pre-B-cell leukaemia transcription factor 4
215540_at	*TCRA*	1·25	1·87	0·67	0·75	T-cell antigen receptor alpha
234440_al	*TCRD*	7·51	1·48	0·50	0·52	Human T-cell receptor delta-chain
Cell growth and maintenance						
213497_at	*ABTB2*	2·06	1·34	0·66	0·63	Ankyrin repeat and BTB (POZ) domain containing 2
201236_s_at	*BTG2*	1·60	1·23	0·60	0·77	BTG family, member 2
235287_at	*CDK6*	1·50	1·32	0·44	0·68	Cyclin-dependent kinase 6
209644_x_at	*CDKN2A*	2·90	1·21	0·67	0·79	Cyclin-dependent kinase inhibitor 2A (melanoma, p16, inhibits CDK4)
236313_at	*CDKN2B*	3·24	1·28	0·58	0·72	Cyclin-dependent kinase inhibitor 2B (p15, inhibits CDK4)
241984_at	*CHES1*	1·38	1·34	0·66	0·63	Checkpoint suppressor 1
202552_s_at	CRIM1	1·94	1·39	0·32	0·61	Cysteine-rich transmembrane BMP regulator 1 (chordin-like)
204844_at	*ENPEP*	1·64	1·75	0·09	0·36	Glutamyl aminopeptidase (aminopeptidase A)
205418_at	*FES*	1·39	1·80	0·61	0·25	Feline sarcoma oncogene
228572_at	*GRB2*	4·69	1·21	0·79	0·78	Growth factor receptor-bound protein 2
207688_s_at	*INHBC*	1·46	1·25	0·51	0·75	Inhibin, beta C
209744_x_at	*ITCH*	1·30	1·47	0·63	0·70	Itchy homolog E3 ubiquitin protein ligase (mouse)
201548_s_at	*JARID1B*	1·27	1·92	0·73	0·46	Jumonji, AT-rich interactive domain IB (RBP2-like)
203297_s_at	*JARID2*	1·42	1·28	0·54	0·72	Jumonji, AT-rich interactive domain 2
41387_r_at	*JMJD3*	1·82	1·24	0·76	0·65	Jumonji domain containing 3
205569_at	*LAMP3*	2·32	1·24	0·76	0·50	Lysosomal-associated membrane protein 3
214039_s_at	*LAPTM4B*	1·41	1·49	0·49	0·59	Lysosomal-associated protein transmembrane 4 beta
205857_x_at	*MSH3*	1·79	1·28	0·58	0·72	MutS homolog 3 (*E. coli*)
209550_at	*NDN*	3·42	1·38	0·17	0·62	Necdin homolog (mouse)
207943_x_at	*PLAGL1*	1·37	1·43	0·57	0·63	Pleiomorphic adenoma gene-like 1
204748_at	*PTGS2*	1·65	1·78	0·14	0·35	Prostaglandin-endoperoxide synthase 2
201482_at	*QSCN6*	1·32	1·23	0·38	0·77	Quiescin Q6
203743_s_at	*TDG*	1·47	1·23	0·54	0·77	Thymine-DNA glycosylase
204227_s_at	*TK2*	2·12	1·26	0·56	0·74	Thymidine kinase 2, mitochondrial

Table 3. Continued

Affi ID	Gene abbreviation	Fold change CB 1	CB 2	PB 1	PB 2	Gene name
Cytokines and chemokines						
207533_at	*CCL1*	1·67	1·48	0·52	0·49	Chemokine (C-C motif) ligand 1
205099_s_at	*CCR1*	4·70	1·21	0·61	0·79	Chemokine (C-C motif) receptor 1
207681_at	*CXCR3*	1·51	1·33	0·41	0·67	Chemokine (C-X-C motif) receptor 3
211469_s_at	*CXCR6*	1·58	1·95	0·32	0·42	Chemokine (C-X-C motif) receptor 6
206613_at	*IL-18R1*	2·32	1·38	0·61	0·62	Interleukin-18 receptor 1
207072_at	*IL-18RAP*	2·16	1·44	0·46	0·56	Interleukin-18 receptor accessory protein
212657_s_at	*IL-1RN*	1·44	3·12	0·56	0·37	Interleukin 1 receptor
206341_at	*IL-2RA*	1·52	1·27	0·73	0·66	Interleukin-2 receptor alpha
202859_x_at	*IL-8*	1·31	3·75	0·38	0·69	Interleukin-8
202643_s_at	*TNFAIP3*	1·61	1·25	0·67	0·75	Tumour necrosis factor, alpha-induced protein 3
202687_s_at	*TNFSF10*	2·83	1·23	0·67	0·77	Tumour necrosis factor (ligand) superfamily member 10
205599_at	*TRAF1*	2·25	1·32	0·68	0·61	Tumour necrosis factor receptor-associated factor 1
202871_at	*TRAF4*	1·43	1·58	0·57	0·48	Tumour necrosis factor receptor-associated factor 4
206366_x_at	*XCL1*	1·24	2·66	0·46	0·76	Chemokine (C motif) ligand 1
Signal transduction						
210538_s_at	*AIP1*	1·35	1·54	0·65	0·61	Baculoviral IAP repeat-containing 3
209369_at	*ANXA3*	1·39	6·82	0·61	0·05	Annexin A3
1554343_a_at	*BRDG1*	1·45	1·67	0·52	0·55	BCR downstream signalling 1
225946_at	*C12orf2*	3·20	1·77	0·23	0·23	Ras association (RaIGDS/AF-6) domain family 8
204392_at	*CAMK1*	1·26	1·62	0·74	0·54	Calcium/calmodulin-dependent protein kinase I
231042_s_at	*CAMK2D*	1·31	1·63	0·25	0·69	Calcium/calmodulin-dependent protein kinase (CaM kinase) II delta
205692_s_at	*CD38*	1·37	1·29	0·71	0·48	CD38 antigen (p45)
231747_at	*CYSLTR1*	3·16	1·45	0·55	0·43	Cysteinyl leukotriene receptor 1
211272_s_at	*DGKA*	1·43	1·23	0·77	0·54	Diacylglycerol kinase alpha 80 kDa
200762_at	*DPYSL2*	1·35	1·40	0·37	0·65	Dihydropyrimtdinase-like 2
208370_s_at	*DSCR1*	1·23	1·90	0·63	0·77	Down syndrome critical region gene 1
204794_at	*DUSP2*	1·55	2·57	0·39	0·45	Dual specificity phosphatase 2
204015_s_at	*DUSP4*	1·35	2·66	0·65	0·39	Dual specificity phosphatase 4
211333_s_at	*FASLG*	1·20	1·37	0·49	0·80	Fas ligand (TNF superfamily, member 6)
211535_s_at	*FGFR1*	1·23	2·79	0·70	0·77	Fibroblast growth factor receptor 1
224148_at	*FYB*	1·50	1·21	0·45	0·79	FYN binding protein (FYB-120/130)
209304_x_at	*GADD45B*	1·55	1·29	0·65	0·71	Growth arrest and DNA-damage-inducible beta
234284_at	*GNG8*	1·50	3·16	0·50	0·35	Guanine nucleotide binding protein (G protein), gamma 8
224285_at	*GPR174*	1·91	1·42	0·56	0·58	G protein-coupled receptor 174
223767_at	*GPR84*	4·41	1·44	0·05	0·56	G protein-coupled receptor 84
211555_s_at	*GUCY1B3*	1·66	1·73	0·34	0·03	Guanylate cyclase 1, soluble, beta 3
38037_at	*HBEGF*	1·54	1·36	0·55	0·64	Heparin-binding EGF-like growth factor
203820_s_at	*IMP-3*	1·83	2·18	0·17	0·17	IGF-II-mRNA-binding protein 3
203006_at	*INPP5A*	1·40	1·86	0·60	0·52	Inositol polyphosphate-5-phosphatase, 40 kDa
231779_at	*IRAK2*	1·93	1·46	0·46	0·54	Interleukin-1 receptor associated kinase 2
32137_at	*JAG2*	1·58	1·29	0·71	0·64	Jagged 2
203904_x_at	*KAI1*	1·65	1·59	0·41	0·25	CD82 antigen
235252_at	*KSR*	1·72	1·56	0·43	0·44	Kinase suppressor of ras 1
210948_s_at	*LEF1*	1·21	1·64	0·41	0·79	Hypothetical protein LOC641518
203236_s_at	*LGALS9*	1·48	1·27	0·73	0·51	Lectin, galactoside-binding, soluble, 9 (galectin 9)
220253_s_at	*LRP12*	1·27	1·30	0·31	0·73	Low-density lipoprotein-related protein 12
206637_at	*P2RY14*	1·32	1·48	0·39	0·68	Purinergic receptor P2Y, G-protein coupled, 14
210837_s_at	*PDE4D*	1·35	1·31	0·62	0·69	Phosphodiesterase 4D, cAMP-specific
206726_at	*PGDS*	6·45	1·40	0·60	0·43	Prostaglandin D2 synthase, haematopoietic
210617_at	*PHEX*	1·53	4·08	0·21	0·47	Phosphate regulating endopeptidase homologue, X-linked
206370_at	*PIK3CG*	1·23	1·32	0·50	0·77	Phosphoinositide-3-kinase, catalytic, gamma polypeptide
205632_s_at	*PIP5K1B*	1·32	1·42	0·64	0·68	Phosphalidylinositol-4-phosphate 5-kinase, type 1 beta

Table 3. Continued

Affi ID	Gene abbreviation	Fold change CB 1	CB 2	PB 1	PB 2	Gene name
215195_at	*PRKCA*	2·17	1·36	0·64	0·61	Protein kinase C, alpha
210832_x_at	*PTGER3*	4·44	1·47	0·07	0·53	Prostaglandin E receptor 3 (subtype EP3)
1553535_a_at	*RANGAP1*	1·58	1·39	0·58	0·61	Ran GTPase activating protein 1
234344_at	*RAP2C*	1·75	1·26	0·46	0·74	RAP2C, member of RAS oncogene family
223809_at	*RGS18*	2·12	1·67	0·15	0·33	Regulator of G-protein signalling 18
209882_at	*RIT1*	1·74	1·32	0·63	0·68	Ras-like without CAAX 1
209451_at	*TANK*	1·34	1·20	0·42	0·80	TRAF family member-associated NFKB activator
204924_at	*TLR2*	1·60	2·52	0·36	0·40	Toll-like receptor 2
217979_at	*TM4SF13*	1·21	2·47	0·30	0·79	Tetraspanin 13
209263_x_at	*TM4SF7*	2·05	1·41	0·58	0·59	Tetraspanin 4
Transcription						
1566989_at	*ARID1B*	1·42	1·27	0·09	0·73	AT-rich interactive domain 1B (SWIl-like)
203973_s_at	*CEBPD*	3·06	1·51	0·33	0·49	CCAAT/enhancer binding protein (C/EBP), delta
221598_s_at	*CRSP8*	1·60	1·29	0·71	0·68	Cofactor required for Spl transcriptional activation, subunit 8, 34 kDa
205249_at	*EGR2*	1·33	4·27	0·67	0·60	Early growth response 2 (Krox-20 homologue, *Drosophila*)
206115_at	*EGR3*	1·31	6·15	0·69	0·48	Early growth response 3
201328_at	*ETS2*	1·57	1·72	0·43	0·40	V-ets erythroblastosis virus E26 oncogene homologue 2 (avian)
218810_at	*FLJ23231*	2·13	1·37	0·63	0·63	Zinc finger CCCH-type containing 12A
209189_at	*FOS*	21·56	1·31	0·13	0·69	V-fos FBJ murine osteosarcoma viral oncogene homologue
223408_s_at	*FOXK2*	2·26	1·22	0·48	0·78	Forkhead box K2
202723_s_at	*FOXO1A*	1·47	1·27	0·57	0·73	Forkhead box O1A (rhabdomyosarcoma)
224211_at	*FOXP3*	1·62	1·41	0·59	0·23	Forkhead box P3
207156_at	*HIST1H2AG*	1·73	1·30	0·41	0·70	Histone 1, H2ag
220042_x_at	*HIVEP3*	1·26	1·65	0·74	0·56	Human immunodeficiency virus type I enhancer binding protein 3
207826_s_at	*ID3*	1·34	8·64	0·60	0·66	Inhibitor of DNA binding 3, dominant negative helix-loop-hetix protein
204549_at	*IKBKE*	2·33	1·29	0·71	0·66	Inhibitor of kappa light polypeptide gene enhancer in B cells
219878_s_at	*KLF13*	1·89	1·26	0·34	0·74	Kruppel-like factor 13
207667_s_at	*MAP2K3*	1·33	1·28	0·72	0·57	Mitogen-activated protein kinase kinase 3
201502_s_at	*NFKBIA*	2·31	1·29	0·71	0·57	Nuclear factor of κ light polypeptide gene enhancer in B cells inhibitor
222105_s_at	*NKIRAS2*	1·84	1·21	0·69	0·79	NFKB inhibitor interacting Ras-like 2
204622_x_at	*NR4A2*	1·35	4·31	0·65	0·63	Nuclear receptor subfamily 4, group A, member 2
207978_s_at	*NR4A3*	1·33	3·53	0·62	0·67	Nuclear receptor subfamily 4, group A, member 3
202600_s_at	*NRIPI*	1·86	1·39	0·26	0·61	Nuclear receptor interacting protein 1
216841_s_at	*SOD2*	1·25	1·73	0·36	0·75	Superoxide dismutase 2, mitochondrial
201416_at	*SOX4*	1·53	2·21	0·47	0·38	SRY (sex determining region Y)-box 4
223635_s_at	*SSBP3*	2·12	1·25	0·75	0·62	Single-stranded DNA binding protein 3
206506_s_at	*SUPT3H*	1·47	1·31	0·57	0·69	Suppressor of Ty 3 homologue (*S. cerevisiae*)
221618_s_at	*TAF9L*	1·25	1·49	0·47	0·75	TAF9-like RNA polymerase II
203177_x_at	*TFAM*	1·63	1·23	0·77	0·57	Transcription factor A, mitochondrial
213943_at	*TWIST1*	1·89	3·14	0·04	0·11	Twist homologue 1 (acrocephalosyndactyly 3; Saethre-Chotzen syndrome)
219836_at	*ZBED2*	1·33	4·76	0·67	0·21	Zinc finger, BED-type containing 2
211965_at	*ZFP36L1*	2·02	1·47	0·29	0·53	Zinc finger protein 36, C3H type-like 1
230760_at	*ZFY*	1·41	1·25	0·75	0·02	Zinc finger protein, Y-linked
228854_at	*ZNF145*	3·26	1·21	0·40	0·79	Transcribed locus
235121_at	*ZNF542*	2·68	1·33	0·63	0·67	Zinc finger protein 542

To investigate whether increased expression of the *IL-17* gene is a general feature of PB-derived $CD4^+$ T cells, we also tested *IL-17* gene expression in the above-described additional samples by real-time RT-PCR analysis. As shown in Fig. 6, all of four PB-derived $CD4^+$ T-cell samples revealed significantly increased gene expression of *IL-17* when compared with the CB-derived samples at 1 week. At 2 weeks, however, *IL-17* gene expression in PB-derived $CD4^+$ T cells was diminished while some of the CB-derived $CD4^+$ T cells (such as sample CB 4) exhibited increased *IL-17* gene expression. When the data were analysed statistically, expression of the *IL-17* gene was found to be

Table 4. Genes up-regulated in $CD4^+$ T cells from peripheral blood (PB)

Affi ID	Gene abbreviation	Fold change				Gene name
		CB 1	CB 2	PB 1	PB 2	
Apoptosis						
1553681_a_at	*PRF1*	0·66	0·51	1·41	1·34	Perforin 1 (pore-forming protein)
B- and T-cell development						
224499_s_at	*AICDA*	0·06	0·44	1·56	3·47	Activation-induced cytidine deaminase
205495_s_at	*GNLY*	0·40	0·51	1·49	6·34	Granulysin
217478_s_at	*HLA-DMA*	0·67	0·39	1·33	1·35	Major histocompatibility complex, class II, DM alpha
203932_at	*HLA-DMB*	0·64	0·31	2·02	1·36	Major histocompatibility complex, class II, DM beta
211991_s_at	*HLA-DPA1*	0·50	0·14	1·54	1·50	Major histocompatibility complex, class II, DP alpha 1
212671_s_at	*HLA-DQA1*	0·44	0·23	1·56	2·56	Major histocompatibility complex, class II, DQ alpha 1
211656_x_at	*HLA-DQB1*	0·63	0·48	1·37	7·07	Major histocompatibility complex, class II, DQ beta 1
210982_s_at	*HLA-DRA*	0·58	0·37	1·50	1·42	Major histocompatibility complex, class II, DR alpha
208306_x_at	*HLA-DRB1*	0·51	0·24	1·49	1·61	Major histocompatibility complex, class II, DR beta 3
204670_x_at	*HLA-DRB5*	0·63	0·22	1·47	1·37	Major histocompatibility complex, class II, DR beta 5
211634_x_at	*IGHV1-69*	0·69	0·77	1·23	1·99	Immunoglobulin heavy variable 1–69
211645_x_at	*IgK*	0·15	0·49	1·51	6·62	Immunoglobulin kappa light chain (IGKV)
221651_x_at	*IGKC*	0·46	0·68	1·32	5·57	Immunoglobulin kappa constant
215379_x_at	*IGLC2*	0·62	0·41	1·38	4·26	Immunoglobulin lambda joining 2
209031_at	*IGSF4*	0·50	0·03	2·33	1·50	Immunoglobulin superfamily, member 4
205686_s_at	*CD86*	0·70	0·23	1·30	1·39	CD86 antigen (CD28 antigen ligand 2, B7-2 antigen)
204698_at	*ISG20*	0·68	0·49	1·32	1·64	Interferon stimulated exonuclease gene, 20 kDa
213915_at	*NKG7*	0·72	0·42	1·28	2·31	Natural killer cell group 7 sequence
Cell growth and maintenance						
201334_s_at	*ARHGEF12*	0·74	0·50	1·26	1·96	Rho guanine nucleotide exchange factor (GEF) 12
230292_at	*CHC1L*	0·70	0·56	1·30	2·02	Regulator of chromosome condensation (RCC1)
205081_at	*CRIP1*	0·56	0·73	1·27	1·75	Cysteine-rich protein 1 (intestinal)
31874_at	*GAS2L1*	0·77	0·52	1·23	2·35	Growth arrest-specific 2 like 1
202364_at	*MXI1*	0·43	0·73	1·27	1·44	MAX interactor 1
219304_s_at	*PDGFD*	0·65	0·71	1·29	3·68	Platelet-derived growth factor D
213397_x_at	*RNASE4*	0·64	0·46	1·36	2·21	Ribonuclease, RNase A family, 4
213566_at	*RNASE6*	0·69	0·39	1·49	1·31	Ribonuclease, RNase A family, k6
219077_s_at	*WWOX*	0·40	0·78	1·25	1·22	WW domain containing oxidoreductase
Cytokine and chemokine						
207861_at	*CCL22*	0·76	0·52	1·24	2·47	Chemokine (C–C motif) ligand 22
238750_at	*CCL28*	0·74	0·45	1·26	1·41	Chemokine (C–C motif) ligand 28
1555759_a_at	*CCL5*	0·71	0·23	1·29	1·92	Chemokine (C–C motif) ligand 5
208304_at	*CCR3*	0·50	0·12	1·50	2·35	Chemokine (C–C motif) receptor 3
205898_at	*CX3CR1*	0·30	0·20	1·70	4·16	Chemokine (C–X3–C motif) receptor 1
204533_at	*CXCL10*	0·80	0·16	1·20	2·53	Chemokine (C–X–C motif) ligand 10
219255_x_at	*IL-17RB*	0·73	0·04	1·27	1·29	Interleukin 17 receptor B
206148_at	*IL-3RA*	0·60	0·54	2·46	1·40	Interleukin 3 receptor, alpha (low affnity)
226333_at	*IL-6R*	0·22	0·79	1·21	2·43	Interleukin-6 receptor
206693_at	*IL-7*	0·09	0·54	1·46	5·86	Interleukin-7
Signal transduction						
204497_at	*ADCY9*	0·76	0·40	1·24	2·40	Adenylate cyclase 9
206170_at	*ADRB2*	0·58	0·35	1·42	3·97	Adrenergic, beta-2-, receptor, surface
202096_s_at	*BZRP*	0·50	0·54	1·59	1·46	Benzodiazapine receptor (peripheral)
230464_at	*EDG8*	0·04	0·09	1·91	2·42	Endothelial differentiation, sphingolipid G-protein-coupled receptor 8
223423_at	*GPR160*	0·54	0·68	1·40	1·32	G protein-coupled receptor 160
227769_at	*GPR27*	0·07	0·08	1·92	244	G protein in-coupled receptor 27
210095_s_at	*IGFBP3*	0·27	0·20	1·73	5·25	Insulin-like growth factor binding protein 3
38671_at	*PLXND1*	0·08	0·65	1·35	2·57	Plexin D1
226101_at	*PRKCE*	0·56	0·43	1·72	1·44	Protein kinase C. epsilon
232629_at	*PROK2*	0·01	0·13	1·87	2·09	Prokineticin 2

Table 4. Continued

Affi ID	Gene abbreviation	Fold change CB 1	CB 2	PB 1	PB 2	Gene name
203329_at	*PTPRM*	0·36	0·62	1·38	1·93	Protein tyrosine phosphatase, receptor type, M
204731_at	*TGFBR3*	0·78	0·55	1·22	2·04	Transforming growth factor, beta receptor III (betaglycan, 300 kDa)
Transcription						
203129_s_at	*KIF5C*	0·67	0·09	1·33	3·43	Kinesin family member 5C
213906_at	*MYBL1*	0·75	0·51	1·25	3·63	V-myb myeloblastosis viral oncogene homologue (avian)-like 1
209815_at	*PTCH*	0·59	0·27	1·41	4·17	Patched homologue (*Drosophila*)
213891_s_at	*TCF4*	0·74	0·65	2·06	1·26	Transcription factor 4
238520_at	*TRERFI*	0·70	0·77	1·23	2·30	Transcriptional regulating factor 1
203603_s_at	*ZFHX1B*	0·74	0·61	1·26	3·63	Zinc finger homobox 1b
213218_at	*ZNF187*	0·74	0·69	1·26	1·76	Zinc finger protein 187
221123_x_at	*ZNF395*	0·38	0·71	1·63	1·29	Zinc finger protein 395

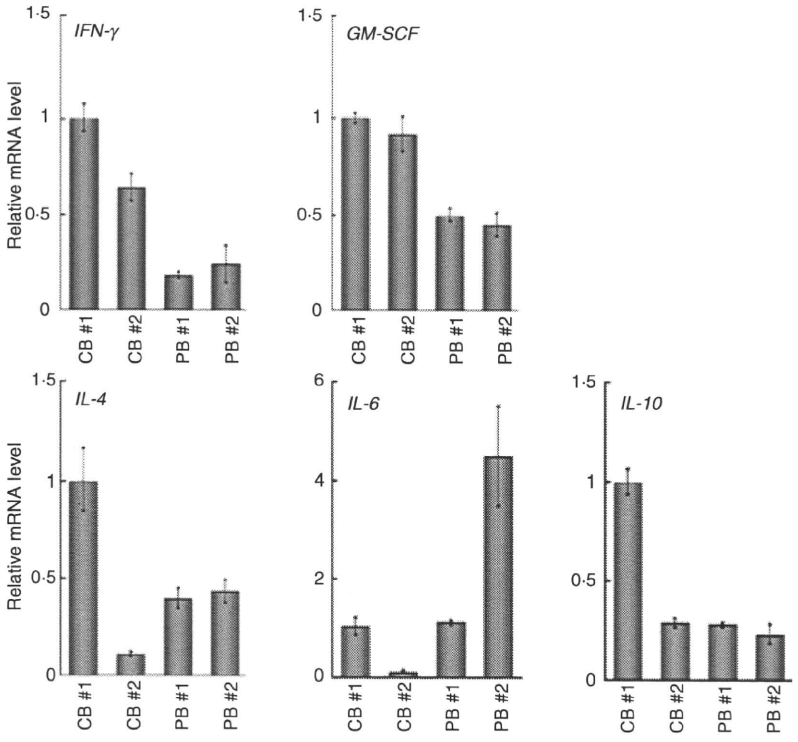

Figure 2. Quantitative polymerase chain reaction (PCR) analysis of the genes related to the T helper type 1 (Th1) and Th2 phenotypes. The expression of the genes indicated was examined by real-time reverse transcriptase (RT)-PCR using the same sample specimens as in Fig 1. Data are normalized to the mRNA level in PB 1 which is arbitrarily set to 1. The signal intensity was normalized using that of a control housekeeping gene [the human glyceraldehyde-3-phosphate dehydrogenase (*GAPDH*) gene]. Data are relative values with the standard deviation (SD) for triplicate wells.

significantly higher in PB-derived $CD4^+$ T cells in comparison with equivalent CB-derived $CD4^+$ T cells at 1 week ($P < 0·05$) but not at 2 weeks (Fig. 6).

Discussion

Although it is generally believed that there are functional differences between CB and PB lymphocytes, the details are obscure. For instance, Azuma *et al.*[13] reported that the phenotype and function of expanded CB lymphocytes were essentially equivalent to those of expanded PB lymphocytes when evaluated in *in vitro* experiments. In the present study, however, we have shown that CB-derived $CD4^+$ T cells revealed a distinct expression profile of genes important for the function of particular T-cell subsets compared with PB-derived $CD4^+$ T cells.

$CD4^+$ T cells can be classified into distinct subsets, including effector $CD4^+$ cells and Tregs, according to their functional characteristics as well as differentiation profiles.[14–16] Typically, effector $CD4^+$ T cells have been further divided into two distinct lineages on the basis of their cytokine production profiles, namely Th1 and Th2. Th1 cells producing cytokines such as IL-2, IFN-γ and GM-CSF have evolved to enhance the eradication of intracellular pathogens and are thought to be potent activators of cell-mediated immunity. In contrast, Th2

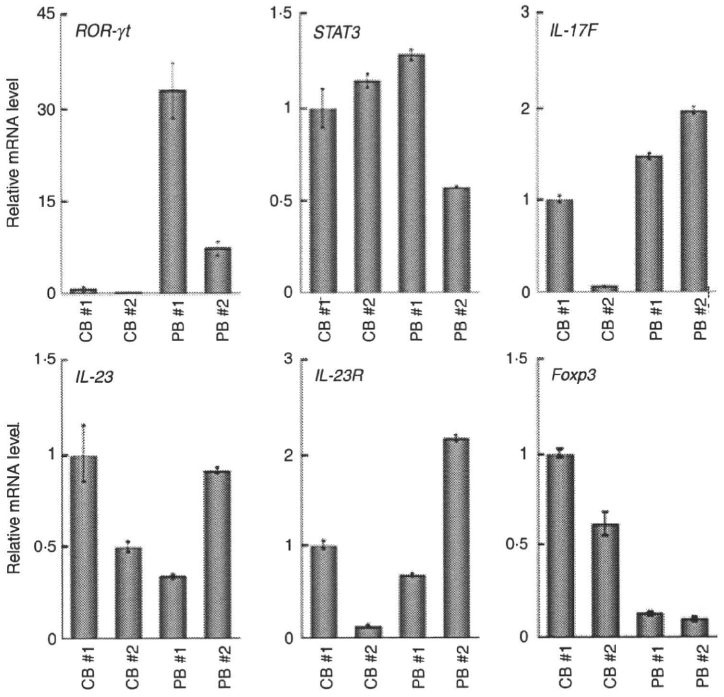

Figure 3. Quantitative polymerase chain reaction (PCR) analysis of the forkhead box protein 3 gene (*FOXP3*) and the genes related to the secretion of interleukin (IL)-17. The expression of the genes indicated was examined as in Fig 2. Data are normalized to the mRNA level in peripheral blood sample 1 (PB 1) as in Fig.2. The signal intensity was normalized using that of a control housekeeping gene [the human glyceraldehyde-3-phosphate dehydrogenase (*GAPDH*) gene]. Data are relative values with the standard deviation for triplicate wells.

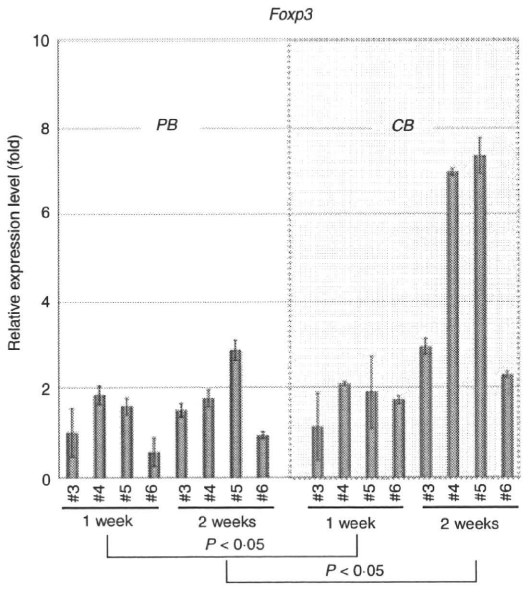

Figure 4. Quantitative polymerase chain reaction (PCR) analysis of the forkhead box protein 3 gene (*FOXP3*) in additional samples. Additional peripheral blood (PB) and cord blood (CB) samples were prepared and RNAs were extracted at 1 and 2 weeks. The expression of the *FOXP3* gene was examined as in Fig. 2. Data are normalized to the mRNA level in the sample of PB 3 at 1 week, which is arbitrarily set to 1. The signal intensity was normalized using that of a control housekeeping gene (the human β-actin gene). Data are relative values with the standard deviation for triplicate wells. The data were analysed statistically and *FOXP3* gene expression in CB-derived $CD4^+$ T cells was found to be significantly higher in comparison with equivalent PB-derived $CD4^+$ T cells at both 1 week ($P < 0{\cdot}05$) and 2 weeks ($P < 0{\cdot}05$).

cells secreting cytokines such as IL-4, IL-5, IL-6, IL-9 and IL-13 have evolved to enhance the elimination of parasitic infections and are thought to be potent activators of B-cell immunoglobulin E production, eosinophil recruitment, and mucosal expulsion. Th1-type responses to self or commensal floral antigens can promote tissue destruction and chronic inflammation, whereas dysregulated Th2-type responses can cause allergy and asthma. The development of Th1 is specified by the transcription factor T-bet (also known as Tbx-21) and master regulators of Th2 differentiation are GATA-3 and c-maf.

As shown in Fig. 2 and Table 2, the gene expression profiles of CB- and PB-derived $CD4^+$ T cells revealed no significant differences regarding cytokines related to the definition of Th1 and Th2, with the exceptions of IFN-γ and GM-CSF. The mRNA levels of IFN-γ and GM-CSF tended to be higher in CB-derived $CD4^+$ T cells than in PB-derived $CD4^+$ T cells. The mRNA expression of the transcription factors T-bet, GATA-3 and c-maf, which regulate Th1 and Th2 cell differentiation, did not differ significantly between CB- and PB-derived $CD4^+$ T cells.

In addition to Th1 and Th2 cells, IL-17 (also known as IL-17A)-producing T lymphocytes have been recently shown to comprise a distinct third subset of T helper cells, termed Th17 cells, in the mouse immune system. Th17 cells exhibit pro-inflammatory characteristics and act as major contributors to autoimmune disease. A number of experiments using animal models support a significant role for IL-17 in the response to allografts.[14,16,17] There is as yet no direct evidence for the existence of discrete Th17 cells in humans, although

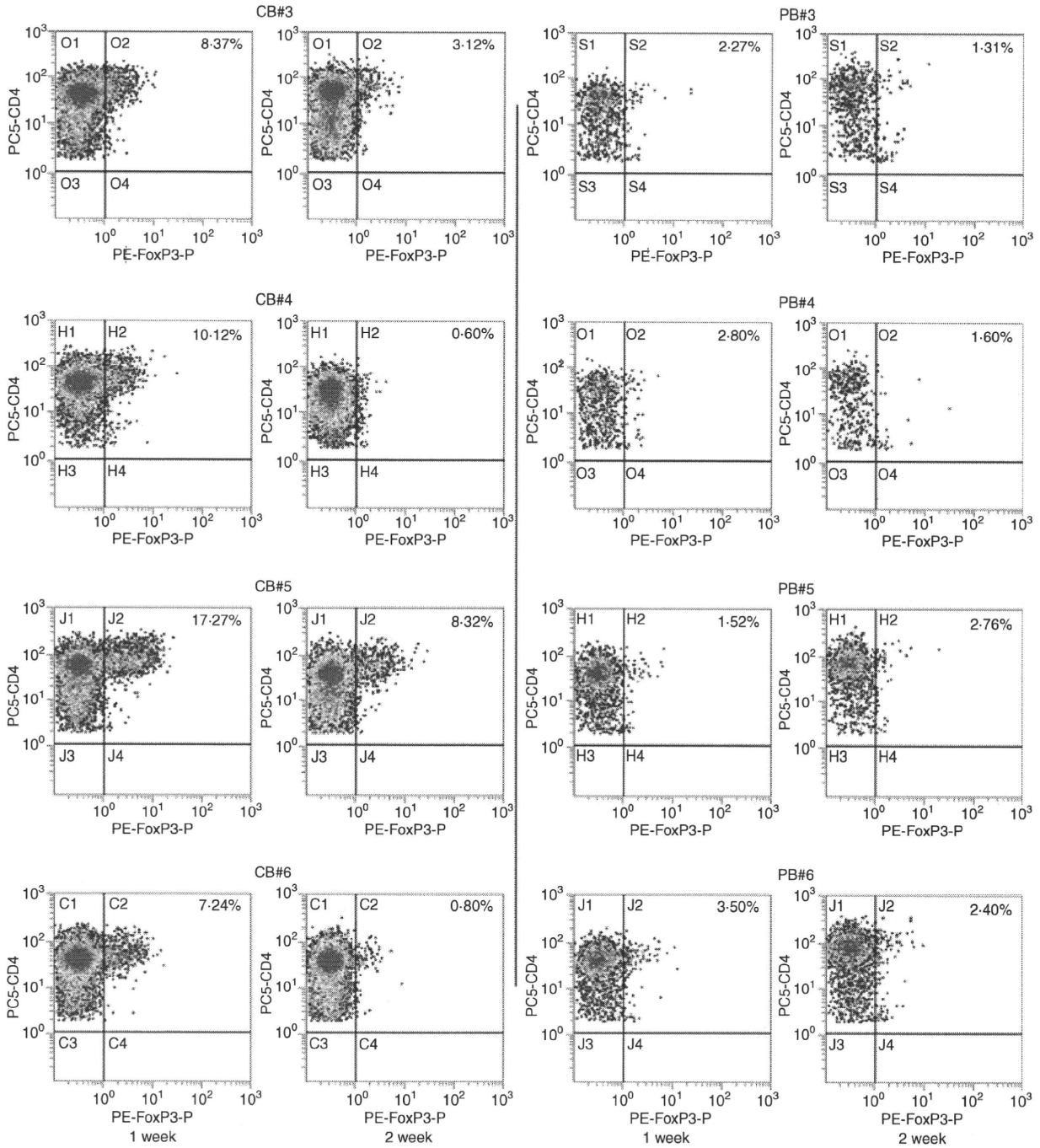

Figure 5. Protein expression of forkhead box protein 3 (Foxp3) in activated $CD4^+$ T cells. The protein expression of Foxp3 in same sample specimens as in Fig. 4 was examined by flow cytometry. The CD4 versus Foxp3 cytogram of the population gated with $CD3^+$ and $CD4^+$ in each sample is presented.

helper T cells secreting IL-17 have clearly been detected in the human immune system.[18] Several studies have shown a correlation between allograft rejection and IL-17. For example, IL-17 levels are elevated in human renal allografts during subclinical rejection and there are detectable mRNA levels in the urinary mononuclear cell sediments of these patients.[19,20] In human lung organ transplantation, IL-17 levels have also been reported to be elevated during acute rejection.[21] Interestingly, in this study, most of the PB-derived $CD4^+$ T-cell samples expressed higher levels of IL-17 mRNA than the CB-derived $CD4^+$ T-cell samples, suggesting that PB-derived $CD4^+$ T cells frequently include potent IL-17-secreting T cells.

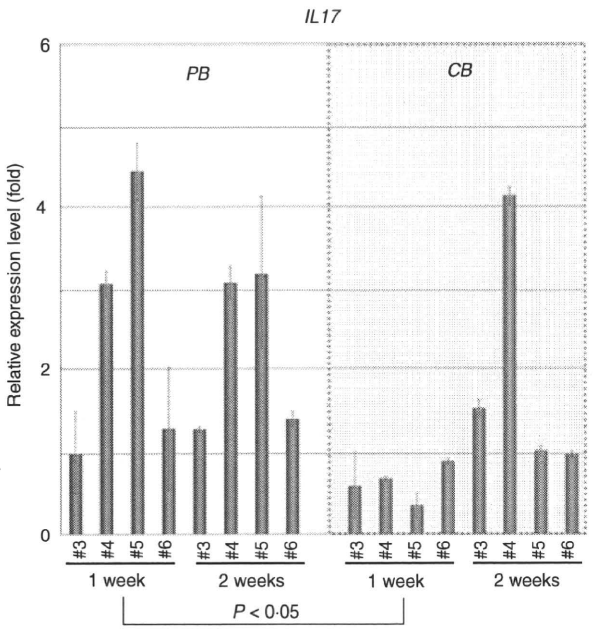

Figure 6. Quantitative polymerase chain reaction (PCR) analysis of interleukin (IL)-17 in additional samples. The expression of the *IL-17* gene in the same sample specimens as in Fig. 4 was examined and presented as in Fig 2. The data were analysed statistically and *IL-17* gene expression in peripheral blood (PB)-derived $CD4^+$ T cells was found to be significantly higher in comparison with equivalent CB-derived $CD4^+$ T cells at 1 week ($P < 0{\cdot}05$) but not at 2 weeks.

Th17 cells expand independently of T-bet or STAT-1. Ivanov *et al.*[22] have shown that the orphan nuclear receptor RORγt is the key transcription factor orchestrating the differentiation of the effector lineage. RORγt induces transcription of the gene encoding IL-17 in naïve $CD4^+$ T helper cells and is required for its expression in response to IL-6 and transforming growth factor (TGF)-β, the cytokines known to induce IL-17 expression. IL-23 is also involved in Th17 cell differentiation, but naïve T cells do not have the IL-23 receptor and are relatively refractory to IL-23 stimulation.[23,24] Although IL-23 seems to be an essential survival factor for Th17 cells, it is not required during their differentiation. It has been suggested that IL-23R expression is up-regulated on RORγt$^+$ Th17 cells in an IL-6-dependent manner. IL-23 may therefore function subsequent to IL-6/TGF-β-induced commitment to the Th17 lineage to promote cell survival and expansion and, potentially, the continued expression of IL-17 and other cytokines that characterize the Th17 phenotype. As presented in Fig. 3, the expression of the *RORγt* gene was significantly weaker in CB-derived $CD4^+$ T cells, whereas the expression of genes encoding IL-23 and the IL-23 receptor did not differ significantly between the $CD4^+$ T cells. Based on the above findings of others, it is possible that the low-level expression of the *RORγt* gene in CB-derived $CD4^+$ T cells is responsible for the absence of *IL-17* mRNA expression in those cells.

Tregs are another functional subset of T cells having anti-inflammatory properties and can cause quiescence of autoimmune diseases and prolongation of transplant function. *In vitro*, Tregs have the ability to inhibit the proliferation and production of cytokines by responder ($CD4^+$ $CD25^-$ and $CD8^+$) T cells subjected to polyclonal stimuli, as well as to down-regulate the responses of $CD8^+$ T cells, NK cells and $CD4^+$ cells to specific antigens.[25,26] These predicates translate *in vivo* to a great number of functions other than the maintenance of tolerance to self-components (prevention of autoimmune disease), such as the ability to prevent transplant rejection. Indeed, donor-specific Tregs can prevent allograft rejection in some models of murine transplant tolerance through a predominant effect on indirect alloresponses.

Foxp3 is thought to be responsible for the development of the Treg population and can act as a phenotypic marker of this fraction.[27] Tregs constitutively express CTLA-4 and there are suggestions that signalling through this pathway may be important for their function, as antibodies to CTLA-4 can inhibit Treg-mediated suppression.[28] As shown above, most of the CB-derived $CD4^+$ T cells were found to express either the *FOXP3* gene or the Foxp3 protein at higher levels compared with PB-derived $CD4^+$ T cells, suggesting that CB-derived $CD4^+$ T cells frequently include a potent Treg population.

As described above, *IL-17* mRNA was more detectable in PB-derived $CD4^+$ cells while *FOXP3* mRNA expression was higher in CB-derived $CD4^+$ cells. Post-transcriptional regulation, as well as differences in mRNA and protein turnover rates, can cause discrepancies between mRNA and protein expression and thus the differences observed in the mRNA expression do not necessary directly indicate those in protein expression.[29] Indeed, we observed some discrepancy between the levels of mRNA and protein with regard to Foxp3 expression in CB-derived $CD4^+$ T cells, as presented above. Nevertheless, changes in mRNA expression are mediated by the alteration of transcriptional regulation, and thus should indicate the differentiation ability of the cells. Therefore, our data indicate that CB-derived $CD4^+$ T cells tend frequently to include potent Tregs, while PB-derived $CD4^+$ T cells tend to include potent IL-17-secreting cells. As described above, DLI with donor CB-derived activated $CD4^+$ T cells is currently becoming established as a routine therapeutic strategy in Japan. It has been proposed that the skewing of responses towards Th17 or Th1 cells and away from Tregs may be responsible for the development and/or progression of autoimmune diseases or acute transplant rejection, and it may thus also be speculated that CB-derived $CD4^+$ T cells are more appropriate for DLI than PB-derived $CD4^+$ T cells.

However, our data also indicate the presence of individual, donor-dependent variations in the characteristics of activated $CD4^+$ T cells derived from CB and PB. More-

over, activated $CD4^+$ T cells do not consist of a single population and should include several distinct functional subsets of $CD4^+$ T cells. Therefore, it is important to clarify the characteristics of activated $CD4^+$ T cells in each preparation to predict the therapeutic effect of DLI in each clinical case.

In summary, our findings demonstrate a difference in gene expression between activated $CD4^+$ T cells derived from CB and those derived from PB. The higher level of *FOXP3* gene expression and the lower level of *IL-17* gene expression in CB-derived $CD4^+$ T cells may indicate that these cells have potential as immunomodulators in DLI therapy. Further detailed analysis should reveal the advantages of activated $CD4^+$ T cells from CB in DLI.

Acknowledgements

We thank the Tokyo Cord Blood Bank for the distribution of cord blood for research use. This work was supported by a grant from the Japan Health Sciences Foundation for Research on Publicly Essential Drugs and Medical Devices (KHC2032), Health and Labour Sciences Research Grants (the 3rd term comprehensive 10-year strategy for cancer control H19-010, Research on Children and Families H18-005, Research on Human Genome Tailor-made and Research on Publicly Essential Drugs and Medical Devices H18-005), and a Grant for Child Health and Development from the Ministry of Health, Labour and Welfare of Japan. It was also supported by CREST, JST.

Disclosures

No competing personal or financial interests exist for any of the authors in relation to this manuscript.

References

1 Loren AW, Porter DL. Donor leukocyte infusions after unrelated donor hematopoietic stem cell transplantation. *Curr Opin Oncol* 2006; **18**:107–14.

2 Roush KS, Hillyer CD. Donor lymphocyte infusion therapy. *Transfus Med Rev* 2002; **16**:161–76.

3 Alyea EP, Soiffer RJ, Canning C *et al.* Toxicity and efficacy of defined doses of CD4(+) donor lymphocytes for treatment of relapse after allogeneic bone marrow transplant. *Blood* 1998; **91**:3671–80.

4 Giralt S, Hester J, Huh Y *et al.* CD8-depleted donor lymphocyte infusion as treatment for relapsed chronic myelogenous leukemia after allogeneic bone marrow transplantation. *Blood* 1995; **86**:4337–43.

5 Tomizawa D, Aoki Y, Nagasawa M *et al.* Novel adopted immunotherapy for mixed chimerism after unrelated cord blood transplantation in Omenn syndrome. *Eur J Haematol* 2005; **75**:441–4.

6 Cohena Y, Nagler A. Hematopoietic stem-cell transplantation using umbilical-cord blood. *Leuk Lymphoma* 2003; **44**:1287–99.

7 Parmar S, Robinson SN, Komanduri K *et al.* Ex vivo expanded umbilical cord blood T cells maintain naive phenotype and TCR diversity. *Cytotherapy* 2006; **8**:149–57.

8 Robinson KL, Ayello J, Hughes R, van de Ven C, Issitt L, Kurtzberg J, Cairo MS. Ex vivo expansion, maturation, and activation of umbilical cord blood-derived T lymphocytes with IL-2, IL-12, anti-CD3, and IL-7. Potential for adoptive cellular immunotherapy post-umbilical cord blood transplantation. *Exp Hematol* 2002; **30**:245–51.

9 Miyagawa Y, Okita H, Nakaijima H *et al.* Inducible expression of chimeric EWS/ETS proteins confers Ewing's family tumor-like phenotypes to human mesenchymal progenitor cells. *Mol Cell Biol* 2008; **28**:2125–37.

10 Werlen G, Hausmann B, Naeher D, Palmer E. Signaling life and death in the thymus: timing is everything. *Science* 2003; **299**:1859–63.

11 Riley JL, June CH. The CD28 family: a T-cell rheostat for therapeutic control of T-cell activation. *Blood* 2005; **105**:13–21.

12 Woo EY, Yeh H, Chu CS, Schlienger K, Carroll RG, Riley JL, Kaiser LR, June CH. Cutting edge: regulatory T cells from lung cancer patients directly inhibit autologous T cell proliferation. *J Immunol* 2002; **168**:4272–6.

13 Azuma H, Yamada Y, Shibuya-Fujiwara N *et al.* Functional evaluation of ex vivo expanded cord blood lymphocytes: possible use for adoptive cellular immunotherapy. *Exp Hematol* 2002; **30**:346–51.

14 Afzali B, Lombardi G, Lechler RI, Lord GM. The role of T helper 17 (Th17) and regulatory T cells (Treg) in human organ transplantation and autoimmune disease. *Clin Exp Immunol* 2007; **148**:32–46.

15 Castellino F, Germain RN. Cooperation between CD4+ and CD8+ T cells: when, where, and how. *Annu Rev Immunol* 2006; **24**:519–40.

16 Reiner SL. Development in motion: helper T cells at work. *Cell* 2007; **129**:33–6.

17 Bi Y, Liu G, Yang R. Th17 cell induction and immune regulatory effects. *J Cell Physiol* 2007; **211**:273–8.

18 Fossiez F, Djossou O, Chomarat P *et al.* T cell interleukin-17 induces stromal cells to produce proinflammatory and hematopoietic cytokines. *J Exp Med* 1996; **183**:2593–603.

19 Loong CC, Hsieh HG, Lui WY, Chen A, Lin CY. Evidence for the early involvement of interleukin 17 in human and experimental renal allograft rejection. *J Pathol* 2002; **197**:322–32.

20 Van Kooten C, Boonstra JG, Paape ME *et al.* Interleukin-17 activates human renal epithelial cells in vitro and is expressed during renal allograft rejection. *J Am Soc Nephrol* 1998; **9**:1526–34.

21 Vanaudenaerde BM, Dupont LJ, Wuyts WA *et al.* The role of interleukin-17 during acute rejection after lung transplantation. *Eur Respir J* 2006; **27**:779–87.

22 Ivanov II, McKenzie BS, Zhou L, Tadokoro CE, Lepelley A, Lafaille JJ, Cua DJ, Littman DR. The orphan nuclear receptor RORgammat directs the differentiation program of proinflammatory IL-17+ T helper cells. *Cell* 2006; **126**:1121–33.

23 Langrish CL, Chen Y, Blumenschein WM *et al.* IL-23 drives a pathogenic T cell population that induces autoimmune inflammation. *J Exp Med* 2005; **201**:233–40.

24 Oppmann B, Lesley R, Blom B *et al.* Novel p19 protein engages IL-12p40 to form a cytokine, IL-23, with biological activities similar as well as distinct from IL-12. *Immunity* 2000; **13**: 715–25.

25 Dieckmann D, Plottner H, Berchtold S, Berger T, Schuler G. Ex vivo isolation and characterization of CD4(+) CD25(+) T cells with regulatory properties from human blood. *J Exp Med* 2001; **193**:1303–10.

26 Wing K, Lindgren S, Kollberg G, Lundgren A, Harris RA, Rudin A, Lundin S, Suri-Payer E. CD4 T cell activation by myelin oligodendrocyte glycoprotein is suppressed by adult but not cord blood CD25+ T cells. *Eur J Immunol* 2003; **33**:579–87.

27 Wan YY, Flavell RA. Identifying Foxp3-expressing suppressor T cells with a bicistronic reporter. *Pro Natl Acad Sci USA* 2005; **102**:5126–31.

28 Read S, Greenwald R, Izcue A, Robinson N, Mandelbrot D, Francisco L, Sharpe AH, Powrie F. Blockade of CTLA-4 on CD4+ CD25+ regulatory T cells abrogates their function in vivo. *J Immunol* 2006; **177**:4376–83.

29 Hack CJ. Integrated transcriptome and proteome data: the challenges ahead. *Brief Funct Genomic Proteomic* 2004; **3**:212–9.

Journal of Pathology
J Pathol 2010; **221**: 164–174
Published online 18 February 2010 in Wiley InterScience
(www.interscience.wiley.com) DOI: 10.1002/path.2699

ORIGINAL PAPER

Interleukin-2 induces NF-κB activation through BCL10 and affects its subcellular localization in natural killer lymphoma cells

Ka-Kui Chan,[1] Lijun Shen,[1] Wing-Yan Au,[2] Hiu-Fung Yuen,[1] Kai-Yau Wong,[1] Tianhuan Guo,[1] Michelle LY Wong,[1] Norio Shimizu,[3] Junjiro Tsuchiyama,[4] Yok-Lam Kwong,[2] Raymond HS Liang[2] and Gopesh Srivastava[1]*

[1] *Department of Pathology, The University of Hong Kong, Queen Mary Hospital, Hong Kong, China*
[2] *Department of Medicine, The University of Hong Kong, Queen Mary Hospital, Hong Kong, China*
[3] *Medical Research Institute, Tokyo Medical and Dental University, Tokyo, Japan*
[4] *Department of Pathology, Kawasaki Medical School, Kurashiki, Okayama, Japan*

**Correspondence to: Gopesh Srivastava, Lymphoma Research Laboratory, Department of Pathology, The University of Hong Kong, Queen Mary Hospital, Pokfulam, Hong Kong, China. e-mail: gopesh@pathology.hku.hk*

Abstract

Deregulation of nuclear factor (NF)-κB signalling is common in cancers and is essential for tumourigenesis. Constitutive NF-κB activation in extranodal natural killer (NK)-cell lymphoma, nasal type (ENKL) is known to be associated with aberrant nuclear translocation of BCL10. Here we investigated the mechanisms leading to NF-κB activation and BCL10 nuclear localization in ENKLs. Given that ENKLs are dependent on T-cell-derived interleukin-2 (IL2) for cytotoxicity and proliferation, we investigated whether IL2 modulates NF-κB activation and BCL10 subcellular localization in ENKLs. In the present study, IL2-activated NK lymphoma cells were found to induce NF-κB activation via the PI3K/Akt pathway, leading to an increase in the entry of G_2/M phase and concomitant transcription of NF-κB-responsive genes. We also found that BCL10, a key mediator of NF-κB signalling, participates in the cytokine receptor-induced activation of NF-κB. Knockdown of BCL10 expression resulted in deficient NF-κB signalling, whereas Akt activation was unaffected. Our results suggest that BCL10 plays a role downstream of Akt in the IL2-triggered NF-κB signalling pathway. Moreover, the addition of IL2 to NK cells led to aberrant nuclear translocation of BCL10, which is a pathological feature of ENKLs. We further show that BCL10 can bind to BCL3, a transcriptional co-activator and nuclear protein. Up-regulation of BCL3 expression was observed in response to IL2. Similar to BCL10, the expression and nuclear translocation of BCL3 were induced by IL2 in an Akt-dependent manner. The nuclear translocation of BCL10 was also dependent on BCL3 because silencing BCL3 by RNA interference abrogated this translocation. We identified a critical role for BCL10 in the cytokine receptor-induced NF-κB signalling pathway, which is essential for NK cell activation. We also revealed the underlying mechanism that controls BCL10 nuclear translocation in NK cells. Our findings provide insight into a molecular network within the NF-κB signalling pathway that promotes the pathogenesis of NK cell lymphomas. Copyright © 2010 Pathological Society of Great Britain and Ireland. Published by John Wiley & Sons, Ltd.

Keywords: NK cell lymphoma; IL2; nucleus; BCL10; NF-κB

Received 21 August 2009; Revised 4 January 2010; Accepted 3 February 2010

No conflicts of interest were declared.

Introduction

Extranodal natural killer (NK)-cell lymphoma, nasal type (ENKL) is a major NK cell malignancy that occurs in Asia and Central and South America. Most cases are of NK cell origin, exhibiting CD56 but lacking surface CD3 expression [1]. Immunohistochemistry shows that the tumour cells display an activated NK cell phenotype, with the expression of various cytolytic lymphocyte-associated proteins and surface markers [2,3]. Previously, we reported that constitutive nuclear factor (NF)-κB activation is present in ENKLs but not in resting normal NK cells [4]. This phenotype was also strongly associated with another specific molecular feature, the nuclear translocation of BCL10 in ENKL cells ($p = 0.001$). The underlying molecular mechanisms of this disease, however, are still elusive.

The *BCL10* gene was originally identified from the recurrent involvement of t(1;14)(p22;q32) in gastric mucosa-associated lymphoid tissue (MALT) lymphoma and encodes a cytosolic protein composed of 233 amino acids with pro-inflammatory activity [5]. Nuclear translocation of BCL10 occurs frequently in MALT lymphomas with t(1;14)(p22;q32) and t(11;18)(q21;q21) [6], resulting in more BCL10 protein in tumour cells via the overexpression or stabilization of the protein [7,8]. ENKLs do not harbour these chromosomal aberrations; thus, it is not likely that the same mechanism accounts for the presence of nuclear BCL10 in ENKLs. An alternative mechanism responsible for the same feature of nuclear translocation of BCL10 in ENKLs must exist.

BCL10 is a molecular adaptor that mediates canonical NF-κB signalling in T and B lymphocytes [9–11]. It forms a signalosome along with CARMA1 and MALT1 to relay the antigen receptor signals that activate IKKγ [12]. When the IKK complex is activated, the NF-κB inhibitor IκBα is degraded and NF-κB is allowed to enter the nucleus to induce the transcription of numerous NF-κB-responsive genes. Recent studies have shown that rather than cytotoxicity, the selective role of BCL10 mediates cytokine production when ITAM-coupled NK cell receptors are engaged [13,14]. In contrast to the well-characterized antigen receptor-induced NF-κB signalling, the role of BCL10 in cytokine receptor signalling remains elusive.

Cytokine deregulation is closely associated with the pathogenesis of haematological diseases and cytokine expression patterns sometimes have diagnostic value [15,16]. Notably, interleukin-2 (IL2) is a potent cytokine that promotes the proliferation of primary NK cells. In addition, most of the NK cell lines derived from ENKL are IL2-dependent [17–19]. It is conceivable that IL2 is a survival factor for tumour cells. Moreover, IL2 can cause NF-κB activation; however, the link between the IL2 receptor and NF-κB is less clearly defined [20]. The signalling pathways triggered by the IL2 receptor are diverse and include the JAK/STAT, PI3K/Akt, and Ras/MAPK pathways [21,22]. Among these, Akt was shown to regulate the induction of NF-κB in Jurkat cells and act as a stimulatory signal triggered by antigen engagement, which involves BCL10 [23,24]. We examined the role of Akt and BCL10 in ENKL cells in the cytokine receptor-triggered signalling cascades. Tumour necrosis factor-α (TNF-α), another cytokine, has been shown to induce BCL10 nuclear localization in breast cancer cells [25], suggesting that cytokine stimulation may be one of the contributing factors to aberrant nuclear BCL10 expression. We investigated the effect of IL2 stimulation on BCL10 subcellular localization in NK lymphoma cells to demonstrate the underlying molecular mechanisms.

Materials and methods

Cell lines and reagents

The human NK cell lines SNK-6 and NK-YS of ENKL origin [26] were maintained in RPMI 1640 medium (Hyclone, Logan, UT, USA) supplemented with 10% fetal bovine serum, 2 mM L-glutamine, 100 U/ml penicillin, and 100 μg/ml streptomycin. The cells were routinely cultured with a supplement of 100 U/ml recombinant human IL2 (PeproTech, London, UK). Before the experiments, both cell lines were starved of IL2 for 48 h and then treated with IL2 for 4 h, unless otherwise specified. Cycloheximide (CHX) and Akt inhibitor I (Akt-I) (Calbiochem, Merck Biosciences, Darmstadt, Germany) were dissolved in ethanol and dimethyl sulphoxide (DMSO), respectively, and added 30 min before the addition of IL2 in some experiments. The antibodies used in the study are described in the Supporting information, Supplementary Table 1.

Isolation of normal NK cells

Normal NK cells were isolated from the peripheral blood of two healthy volunteers using the Dynal® NK Cell Negative Isolation Kit (Dynal Biotech, Oslo, Norway). The purity of the NK cells was verified by flow cytometry and found to be over 95%. The normal NK cells were cultured under the same conditions as those described above for the NK cell lines.

RT-PCR analysis

Total RNA was extracted using TRIzol reagent (Invitrogen, Carlsbad, CA, USA). The first-strand cDNA was synthesized from 2 μg of RNA using oligo $d(T)_{16}$ and the GeneAmp RNA PCR Kit (Applied Biosystems, Foster City, CA, USA). Semi-quantitative RT-PCR was performed to detect granzyme B, perforin, *BCL3*, and *GAPDH* mRNA transcripts using AmpliTaq Gold polymerase (Applied Biosystems). The primers used are described in the Supporting information, Supplementary Table 2. The sequences of the primers used for quantitative RT-PCR for granzyme B, perforin, and actin mRNA transcripts are described in the Supporting information, Supplementary Table 3. Products were stained with SYBR Green (Molecular Probes, Eugene, OR, USA) and analysed using a 7700 Real-Time PCR System (Applied Biosystems).

Yeast two-hybrid screening

Yeast two-hybrid screening was performed using the Matchmaker Two-Hybrid System 3 (Clontech, Mountain View, CA, USA). The cDNA library was generated from the RNA of SNK-6 cells. Small-scale library transformation and screening were performed, and potential positive colonies were analysed by PCR screening and sequencing. Putative interactions were further confirmed by co-immunoprecipitation from the cell lines.

Co-immunoprecipitation and western blotting

Cells were lysed in RIPA buffer (Santa Cruz Biotechnology, Santa Cruz, CA, USA). Protein concentrations were measured using the Bio-Rad DC Protein Assay Kit (Bio-Rad, Hercules, CA, USA). Proteins were immunoprecipitated with antibodies or isotype-matched immunoglobulin at 4 °C overnight. The bound protein–antibody complexes were pulled down with protein G plus-agarose (Santa Cruz Biotechnology). The products were resolved by 10% SDS-PAGE and transferred to a PVDF membrane. The membrane was blocked with 5% non-fat milk and incubated with the primary antibody at 4 °C overnight or at room temperature for 1 h. After washing with TBST, the membrane was incubated with an HRP-conjugated secondary antibody for 1 h at room temperature. Signals were detected using Hyperfilm with ECL plus reagent (Amersham Biosciences, Piscataway, NJ, USA).

Cellular fractionation

Cells were lysed with 10 mM HEPES containing 1.5 mM $MgCl_2$, 10 mM KCl, 0.5 mM DTT, 0.5 mM PMSF, and 0.2% Nonidet P-40 supplemented with a cocktail of protease inhibitors. Lysates were placed on ice for 10 min and separated by centrifugation at 3000 rpm for 10 min. The supernatant was collected as the cytoplasmic fraction and the cell pellet was further lysed with buffer containing 50 mM Tris (pH 8.0), 500 mM NaCl, 5 mM EDTA, 0.5 mM DTT, 0.5 mM PMSF, 1% Nonidet P-40, and protease inhibitors at 4 °C for 30 min. The supernatant was collected as the nuclear fraction following centrifugation at 13 000 rpm for 10 min at 4 °C.

Electromobility shift assay (EMSA)

The NF-κB oligonucleotide consensus probe and gel shift assay system were purchased from Promega (Madison, WI, USA). The oligonucleotide was labelled with [γ-^{32}P]ATP using a T4 polynucleotide kinase and the unincorporated radionucleotides were removed using MicroSpin G25 columns. Cells were harvested and nuclear protein fractions were collected. Equal amounts of nuclear extracts were incubated with the radioactive probe according to the user manual. For the supershift assay, antibodies against p50 or p65 were added to the reaction mixture and incubated at 4 °C for 1 h. The DNA–protein complexes were resolved in a 5% polyacrylamide gel. The gel was then dried and exposed to X-ray film at −70 °C.

RNA interference with shRNA

Complementary oligonucleotides (Supporting information, Supplementary Table 4) were annealed and ligated with the pSIREN-RetroQ vector using the knockout RNAi system (Clontech). A negative control shRNA oligonucleotide against luciferase (shCon) was provided by the RNAi system. Transfection of the packaging cell line, PT67, was performed using FuGene 6 transfection reagent (Roche, Mannheim, Germany). The medium containing the viral particles was collected 2 days after transfection. The supernatant was filtered through a 0.45 μm filter and polybrene (8 μg/ml) (Sigma-Aldrich, St. Louis, MO, USA) was then added. SNK-6 cells were incubated with the virus-containing supernatant for 24 h and the supernatant was replaced with fresh RPMI medium. Infected cells were collected 1 day later.

Flow cytometry

Cells were collected by centrifugation and washed twice with PBS. The cell pellets were fixed overnight with ice-cold 70% ethanol and the cells were then resuspended in PBS containing 200 μg/ml RNase A and 20 μg/ml propidium iodide (Sigma-Aldrich). The samples were examined using a FACS Calibur flow cytometer (BD Bioscience, San Jose, CA, USA) and the Cell Quest program. Proportions of cells in different phases were quantified with ModFit LT software (Verity Software House, Topsham, ME, USA).

Immunofluorescence microscopy

Cells were collected and cytospun onto slides. After fixation with cold methanol, the slides were incubated with the primary antibody at 4 °C overnight. After washing, a fluorescein isothiocyanate (FITC)-conjugated secondary antibody (Chemicon, Temecula, CA, USA) was applied to the slides. Cell nuclei were counterstained with 4′,6-diamidino-2-phenylindole (DAPI; Roche) and signals were visualized using an Eclipse E800M microscope (Nikon, Tokyo, Japan).

Statistics

The data were compared using the t-test and $p < 0.05$ was regarded to be statistically significant.

Results

IL2 induces NF-κB activation via Akt

To determine whether PI3K and Akt were engaged in IL2-induced NF-κB signalling, two bona fide ENKL cell lines, SNK-6 and NK-YS [26], were treated with IL2 prior to analysis. IL2 stimulation resulted in the binding of NF-κB to its consensus sequences, as shown by the EMSA (Figure 1a), which demonstrated that IL2 activates NK tumour cells via the canonical NF-κB pathway involving the p65/p50 heterodimer. Consistently, more of the p65 subunit was detected in nuclear extracts from ENKL cells grown in the presence of IL2, while its cytosolic counterpart was unchanged (Figure 1b).

To address the role of Akt in this process, we treated the cells with an Akt-specific inhibitor (Akt-I) [27] before the addition of IL2. Akt-I is a phosphatidylinositol ether analogue that binds to the pleckstrin homology domain of Akt. We used a dosage of Akt-I that does not affect cell viability or PI3K (IC_{50} = 83 μM), such that other PI3K-related downstream signalling molecules remained unaffected. The addition of Akt-I inhibited the nuclear translocation of p65 and the binding of NF-κB to its consensus sequences (Figures 1a and 1b). To demonstrate the specific effect of this inhibitor on Akt activity, we examined the phosphorylation status of the Ser^{473} residue, a hallmark of Akt activation. As expected, Akt phosphorylation was increased in the cells treated with IL2 alone, whereas treatment of the cells with Akt-I for 4 h suppressed IL2-induced Akt phosphorylation (Figure 1c).

To evaluate NF-κB activity further under these conditions, semi-quantitative RT-PCR was performed to examine the RNA transcript levels of granzyme B and perforin. Granzyme B and perforin are the two major components of NK cell cytolytic granules and their genes are responsive to NF-κB [20,28]. The RT-PCR results showed that IL2 enhances the transcription

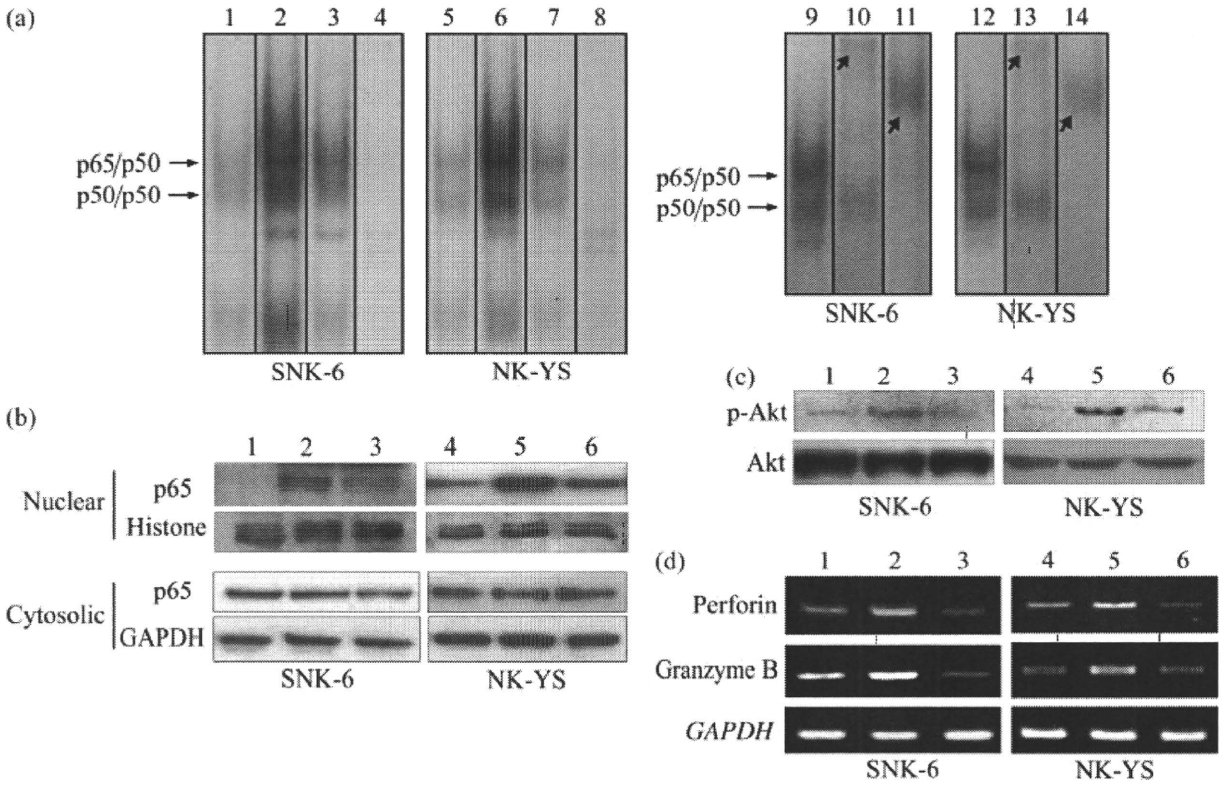

Figure 1. Activation of NF-κB via Akt. (a) EMSA results of NK cell lines SNK-6 and NK-YS. Cells were deprived of IL2 (1 and 5) or treated with 300 U/ml of IL2 alone (2, 6, 9, and 12) or IL2 together with 10 μM Akt-I (3 and 7). In the supershift assay, nuclear lysates were incubated with either p65 antibody (10 and 13) or p50 antibody (11 and 14) to identify the position (short-tailed arrows) of the p65/p50 heterodimer and the p50 homodimer. A cold competitor of the NF-κB consensus sequence was added as a control (4 and 8). (b) Immunoblotting results for p65 in nuclear and cytosolic extracts from the SNK-6 and NK-YS cell lines. GAPDH was used for the normalization of cytosolic proteins and histone H1 was used for the normalization of nuclear proteins. (c) Immunoblotting results for phospho-Akt (Ser^{473}), with total Akt used as the normalization control. (d) Semi-quantitative RT-PCR results for perforin and granzyme B. *GAPDH* was used for normalization. For b, c, and d, cells were deprived of IL2 (1 and 4) or treated with 300 U/ml IL2 alone (lanes 2 and 5) or IL2 together with 10 μM Akt-I (lanes 3 and 6).

of granzyme B and perforin, whereas Akt-I blocked this effect (Figure 1d).

IL2-induced NF-κB activation is BCL10-dependent

To explore the potential role of BCL10 in cytokine receptor signalling, the expression of BCL10 was knocked down using an shRNA specifically targeting BCL10. As demonstrated by western blot, sequence B suppressed BCL10 expression more effectively than sequence A (Figure 2a). Depletion of BCL10 rendered the SNK-6 cells less responsive to IL2 with regard to NF-κB activation, compared with treatment with the control sequence (Figure 2b). To rule out off-target silencing effects on Akt activation due to the shRNA, we again measured the levels of Akt phosphorylation in cells treated with shRNA. As shown in Figure 2c, no remarkable changes in Akt phosphorylation levels were observed between the mock control and the shRNA-treated cells. These results suggest that BCL10 participates in IL2-mediated NF-κB signalling and likely plays a role downstream of Akt.

We then examined the transcription of the cytolytic genes perforin and granzyme B, which is responsive to NF-κB. As expected, depletion of BCL10 resulted

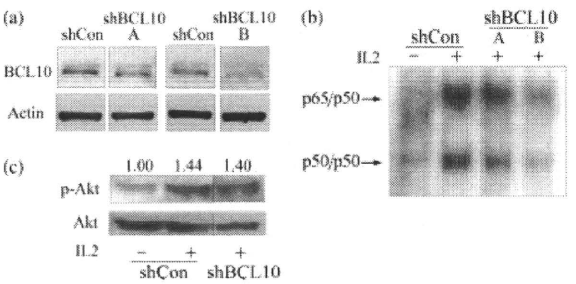

Figure 2. Knockdown of BCL10 expression inhibits IL2-induced NF-κB activation. (a) Immunoblotting results for BCL10 in SNK-6 cells. BCL10 expression was knocked down using two shRNA sequences (shBCL10-A and -B). A luciferase sequence (shCon) was used as a negative control. Actin served as the normalization control for immunoblotting. (b) EMSA results showing the changes in NF-κB activity in SNK-6 cells. (c) Immunoblotting results for phospho-Akt (p-Akt) in SNK-6 cells, with total Akt used as a normalization control. Band density was measured with Grab-IT (Ultra Violet Products Ltd, Cambridge, UK). The p-Akt to Akt ratio is shown at the top of the panel for comparison.

in a decline in the transcription of both perforin and granzyme B (Figure 3a). Furthermore, alterations in NF-κB activity were demonstrated by cell cycle analysis because the up-regulation of NF-κB activity

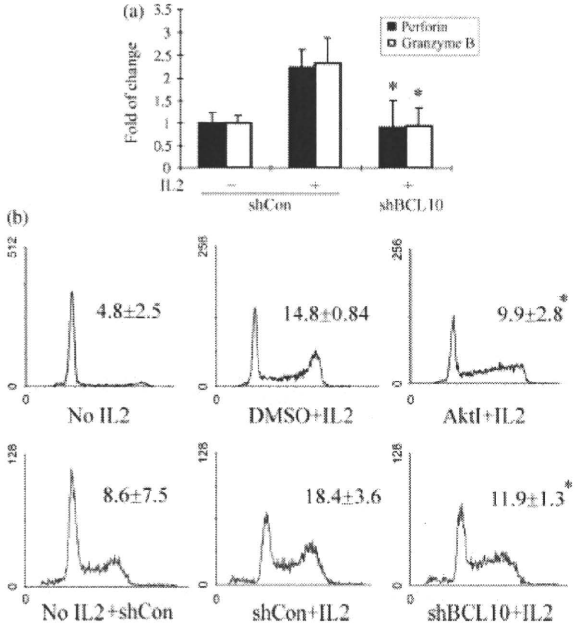

Figure 3. Knockdown of BCL10 suppresses IL2-induced gene transcription and restricts the number of cells in the G_2/M phase. (a) Quantitative RT-PCR results for perforin and granzyme B in SNK-6 cells. shRNA-transduced cells were treated in the presence or absence of IL2 as specified in the figure. (b) Blocking Akt or silencing BCL10 with shRNA reduced the percentage of SNK-6 cells in the G_2/M phase. DMSO was the vehicle control for Akt-I. A luciferase sequence (shCon) was used as a negative control for RNA interference in a and b. Each histogram is representative of three independent experiments. The percentage of cells in the G_2/M phase from three experiments is shown as the mean ± SD (*$p < 0.05$ when compared with the corresponding negative or vehicle control).

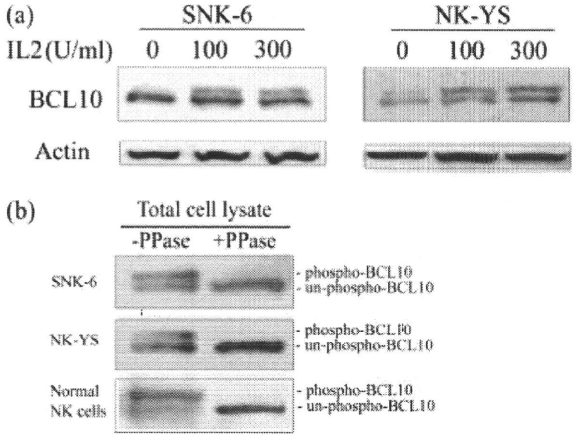

Figure 4. IL2 induces an increase in the total and phosphorylated forms of BCL10. (a) Immunoblotting results for BCL10 in NK cell lines treated with different concentrations of IL2. β-Actin served as the loading control. (b) Identification of phospho-BCL10 by phosphatase (λ-PPase) treatment and immunoblotting. Total cell lysates were incubated in the presence or absence of phosphatase for 4 h before western blotting.

usually allows more cells to undergo cell division [29]. The addition of IL2 induced more SNK-6 cells to enter the cell cycle, with an increase in the percentage of cells in the G_2/M phase, but this effect could be suppressed by either Akt-I or shBCL10-B (Figure 3b).

IL2 promotes the overexpression and phosphorylation of BCL10

The *BCL10* gene has been suggested to be responsive to NF-κB [25]; we therefore examined the expression level of BCL10 in both cell lines treated with different concentrations of IL2. Incubation with IL2 for 4 h could either increase the total expression level or promote the phosphorylation of BCL10, but the results were slightly different between the two cell lines (Figure 4). In SNK-6 cells, there was an increase in the phosphorylated form of BCL10, but changes in the unphosphorylated form were not evident. In NK-YS cells, both forms seemed to be increased simultaneously along with IL2 in a dose-dependent manner.

IL2 induces BCL10 translocation to the nucleus

In addition to up-regulation of BCL10, IL2 stimulation could trigger the nuclear translocation of BCL10 in NK cells. The malignant cell lines (SNK-6 and NK-YS) and normal NK cells were cultured without the addition of IL2 for 2 days before they were stimulated with IL2. The addition of IL2 resulted in more BCL10 in the nucleus compared with the IL2-deprived cells. This phenomenon was observed not only in both ENKL cell lines, but also in IL2-activated NK cells from healthy individuals; thus, it was a result of the activation of NK cells rather than a lymphoma-specific effect. The BCL10 in the nucleus formed large granules with irregular shapes (Figure 5a). Moreover, the western blot results were consistent with the finding that BCL10 levels increased significantly in nuclear extracts upon IL2 stimulation (Figure 5b), while they increased only slightly in the cytosolic extracts. Like its cytosolic counterpart, nuclear BCL10 was also made up of both phosphorylated and unphosphorylated forms, suggesting that BCL10 phosphorylation alone is not sufficient for nuclear translocation. The nuclear translocation was Akt-dependent, however, as the addition of Akt-I reduced the amount of nuclear BCL10 but did not change that of cytosolic BCL10 (Figure 5c).

BCL3 is a binding partner of BCL10

The translocation of BCL10 has been shown to be aided by another molecule, BCL3, in the human breast carcinoma cell line MCF7 [25] and the diffuse large B-cell lymphoma cell line Pfeiffer [30]. A small-scale yeast two-hybrid screen identified BCL3 as a potential binding partner of BCL10 in our NK tumour cell lines (data not shown). To further confirm the potential interaction between these two molecules, we enriched BCL10 from the crude protein lysates by immunoprecipitation and examined whether BCL3 is a binding partner of BCL10 by western blotting. As shown in Figure 6, the BCL10 antibody was able to

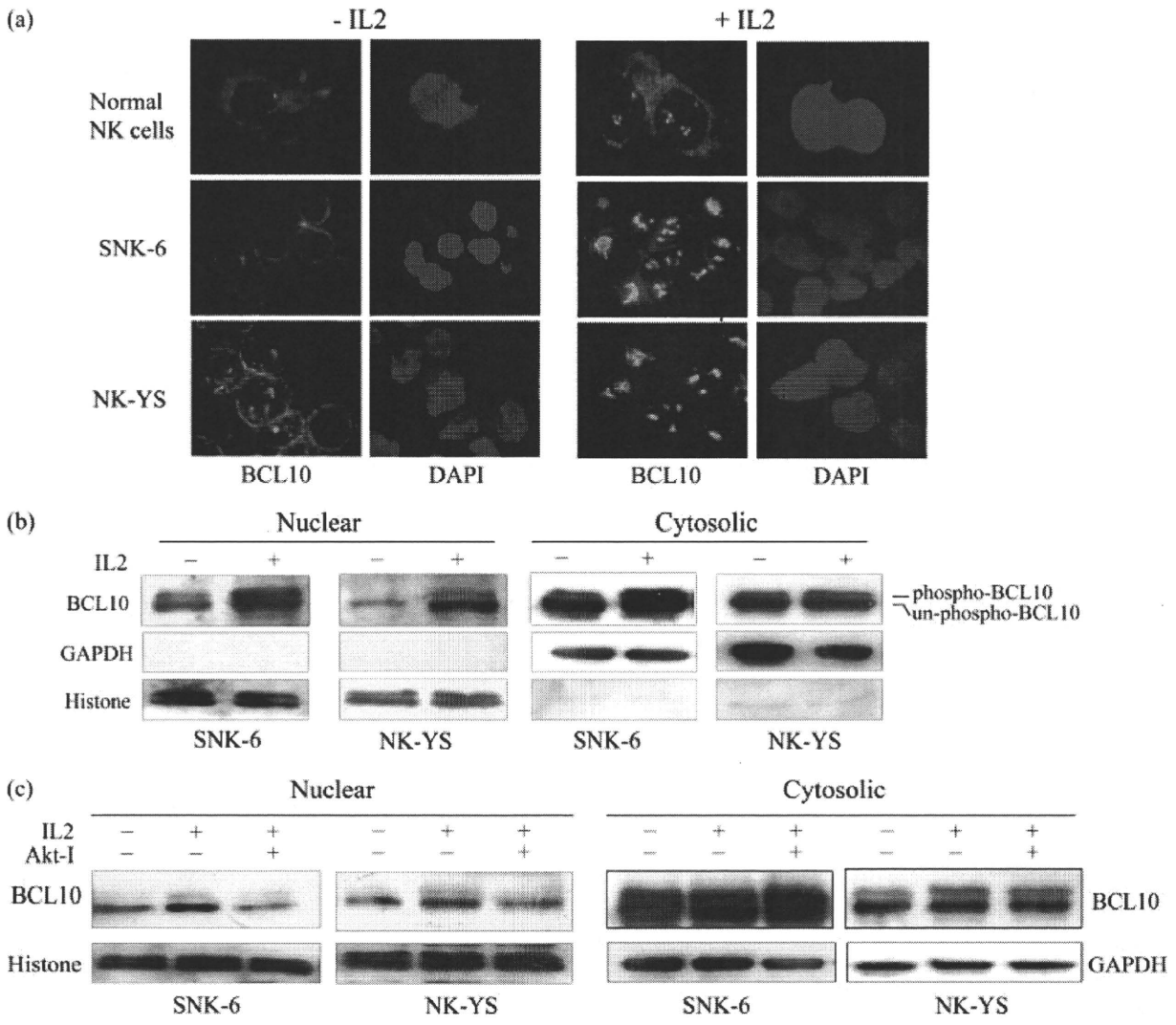

Figure 5. IL2 induces the nuclear translocation of BCL10 in normal and neoplastic NK cells. (a) Immunofluorescence micrographs of the NK-cell cytospin preparations. NK cells were cultured for 24 h in the presence or absence of IL2 (original magnification 400×). BCL10 was detected with a FITC-conjugated antibody (green) and the nuclei were stained with DAPI (blue). (b) Immunoblotting results for BCL10 in protein extracts from subcellular fractionation. GAPDH and histone served as the normalization controls for cytosolic and nuclear proteins, respectively. (c) Immunoblotting results for BCL10 in nuclear and cytosolic extracts from the NK cell lines. The combination of IL2 (300 U/ml) and Akt-I (10 μM) is specified in the figure. GAPDH and histone were used as loading controls for the cytosolic and nuclear extracts, respectively.

co-immunoprecipitate BCL3 in both SNK-6 and NK-YS cells, indicating that they form a complex in these IL2-activated NK cells.

IL2 induces BCL3 overexpression and translocation to the nucleus

We next investigated the molecular response of BCL3 following IL2 stimulation by examining the expression of BCL3 at both the transcriptional and the translational levels. IL2 induced increases in the mRNA and protein levels of BCL3 (Figures 7a and 7b). This effect was again blocked by Akt-I, showing the involvement of the PI3K/Akt pathway (Figure 7c). We next examined whether IL2 could induce the nuclear translocation of BCL3. Western blot analysis showed that more BCL3 was present in both the nuclear and the cytosolic fractions of NK cell lines when they were grown in the presence of IL2 (Figure 7d). Treatment with Akt-I reduced the amount of nuclear and cytosolic BCL3, suggesting that BCL3 expression was affected. Thus, the decrease in the level of nuclear BCL3 must be a result of the down-regulation of BCL3 expression caused by Akt-I.

BCL3 plays a role in the subcellular localization of BCL10

To clarify further the role of BCL3 in the nuclear transfer of BCL10, we used shRNA to suppress the expression of BCL3 and evaluated the subsequent effects on BCL10 subcellular localization. Two sequences targeting *BCL3* mRNA were examined and sequence B was selected to knock down BCL3 expression in

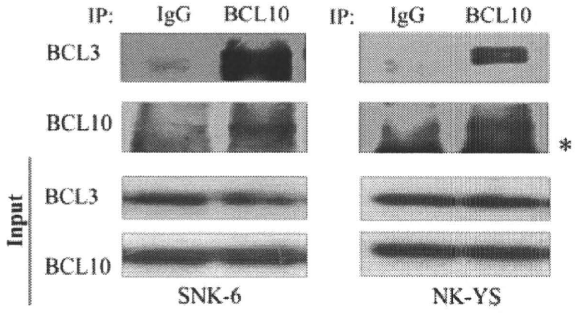

Figure 6. Co-immunoprecipitation of BCL3 with BCL10. An interaction between BCL3 and BCL10 was demonstrated by immunoprecipitation. Whole cell extracts were immunoprecipitated with an anti-BCL10 antibody or isotype-matched IgG (control). The purified product was examined with antibodies against BCL3 and BCL10 by immunoblotting. The asterisk indicates non-specific bands from the immunoglobulin light chains. The 'Input' control shows that the same amount of protein was used for immunoprecipitation.

subsequent experiments (Figure 8a). After infection with the retrovirus carrying the shRNA sequence, SNK-6 cells showed a decrease in BCL3 expression in both the nuclear and the cytosolic extracts. Notably, BCL10 expression decreased along with BCL3 in the nuclear fractions, while cytosolic BCL10 expression remained unchanged (Figure 8b). To identify whether *de novo* protein synthesis is necessary for the translocation, we treated the cells with cycloheximide (CHX), a protein synthesis inhibitor, before stimulation with IL2. This treatment blocked the presence of BCL10 and BCL3 in the nuclear fractions and BCL3 in the cytosolic fractions (Figure 8c). There was a considerable amount of BCL10 in the cytosolic fractions, however, as it is more stable than BCL3. This result suggests that *de novo* synthesis of both BCL10 and BCL3 is necessary for their appearance in the nucleus in response to IL2.

Discussion

Cytokine receptor-induced lymphocyte activation often plays a role in the inflammatory and immune responses that occasionally give rise to lymphomagenesis [31,32]. In low-grade MALT lymphoma, the growth of tumour cells is maintained by stimulating signals from pro-inflammatory cytokines produced during chronic gastritis with persistent infection by *Helicobacter pylori*. Antibiotics that kill *H. pylori* block lymphocyte activation signalling, curing the gastritis and even the MALT lymphoma itself [33,34]. Similarly, ENKL is a lymphoid malignancy associated with Epstein–Barr virus infection [35]. A latent viral product such as LMP1 can up-regulate the expression of different cytokines, including interferon and IL10 [36,37]. Moreover, NK lymphoma cells are functionally active in a cytolytic manner and are characterized by constitutive activation of NF-κB [2], suggesting that cytokine-driven lymphocyte activation is essential for the development of NK cell lymphoma.

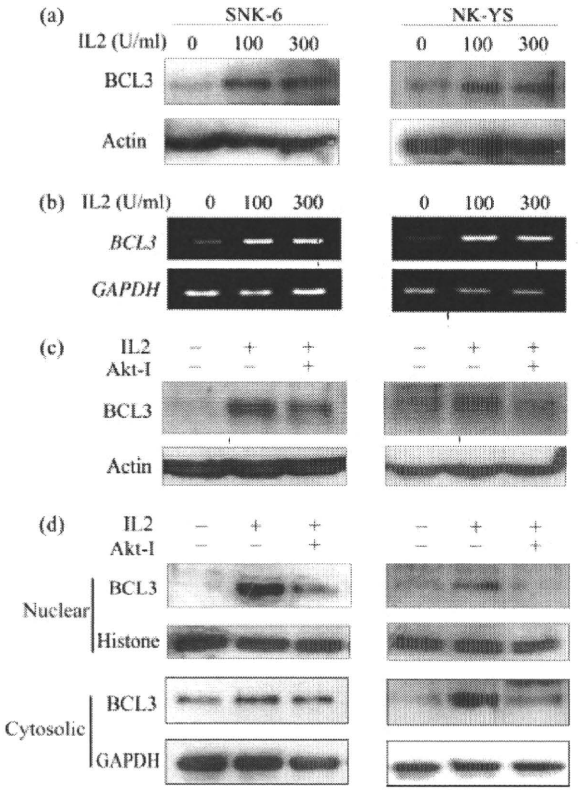

Figure 7. IL2 increases the transcript and protein levels of BCL3. Immunoblotting (a) and RT-PCR results (b) for BCL3 expression in NK cell lines treated with different concentrations of IL2. Actin and GAPDH were used as the normalization controls for a and b, respectively. (c) Immunoblotting results for BCL3 expression. Actin served as the normalization control. (d) Change in the amount of BCL3 in the nuclear and cytosolic extracts. GAPDH and histone were used as loading controls for the cytosolic and nuclear extracts, respectively. For c and d, the combination of IL2 (300 U/ml) or Akt-I (10 μM) is specified in the figure.

With regard to the use of IL2 as a model to study cytokine-driven NF-κB activation, we believe that IL2 is likely among the few cytokines that promote tumourigenesis in NK cell malignancies. It is required to maintain NK cell proliferation *in vitro*, and primary NK cells in human lymph nodes are dependent on T-cell-derived IL2 for cytotoxicity, in addition to viability and proliferation [19]. ENKLs are neoplasms with a cytotoxic NK phenotype [2]. ENKL cells do not express IL2 [38], but reactive T cells in the tumour micro-environment are likely a major source of IL2. Tumour-infiltrating T cells are prevalent in ENKL specimens [39–41] and frequently, they are the major cell population within the primary site and metastases of ENKL [41]. Conceivably IL-2 can be provided by activated T cells *in vivo* in ENKLs.

In the present study, we demonstrated that IL2 triggers NF-κB activation through the Akt pathway. Extensive studies have shown that BCL10 is a key mediator of NF-κB signalling in lymphocytes [42,43]. Along with its conventional role in antigen receptor signalling, recent studies have shown the involvement of BCL10 in mediating NF-κB signalling downstream of G protein-coupled receptors and Toll-like receptors